This article has been accepted for publication in a future issue of this journal, but has not been fully edited. Content may change prior to final publication.
Citation information: DOI10.1109/tmc.2026.3739758, IEEE Transactions on Mobile Computing

Communication-Aware Distributed Control for Cooperative Ramp Merging in Vehicular Networks

Qianju Shen, Qiong Wu, *Senior Member, IEEE,* Pingyi Fan, *Senior Member, IEEE,*
Kezhi Wang, *Senior Member, IEEE,* Wen Chen, *Senior Member, IEEE,*
Cui Zhang, Guoqiang Mao, *Fellow, IEEE*, and Khaled B. Letaief, *Fellow, IEEE*

***Abstract*—Cooperative ramp merging requires reliable coordination among connected vehicles, but practical NR V2X Mode 2 communications may suffer from delay, packet loss, and resource collision due to distributed sidelink resource selection. Existing distributed control methods often assume ideal communication or treat communication impairments as external disturbances, without explicitly linking communication states to vehicle safety constraints. Accordingly, this paper proposes a communication-aware distributed model predictive control (CA-DMPC) framework for cooperative ramp merging. A Markov-chain-based model is developed to characterize NR V2X Mode 2 resource reservation and re-evaluation, including collision persistence, resource reselection, and re-evaluation failure. Predicted communication states are converted into spatial prediction uncertainty and incorporated into MPC safety constraints through an adaptive safety margin. To improve real-time performance, the communication-control optimization problem is decomposed into tractable subproblems, and the vehicle-control component is reformulated as a quadratic programming problem. Simulation results show that the proposed framework achieves smoother control, more stable inter-vehicle spacing, better trajectory tracking, and lower computational cost than benchmark methods.**

***Index Terms*—Ramp Merging, Distributed Control, NR V2X, Resource Re-evaluation, Communication-aware Control.**

I. Introduction

With the growing number of vehicles in urban areas, traffic congestion has become increasingly severe. Among various traffic scenarios, ramp merging is widely recognized as one of the most critical traffic safety scenarios due to frequent vehicle interactions, complex traffic dynamics, and limited maneuvering space [1], [2]. Vehicles on the main road and ramp are required to continuously adjust their speeds and positions to achieve safe merging, which increases driving burden and reduces overall traffic efficiency [3].

To improve the efficiency and safety of ramp merging, early studies mainly investigated cooperative trajectory planning approaches that combined V2X communication with centralized controllers [4], [5]. Although such methods can enhance traffic performance to a certain extent, they require solving global optimization problems and heavily rely on roadside infrastructure support. As a result, centralized control frameworks inherently suffer from limited scalability and restricted real-time capability in large-scale traffic scenarios [6]. To overcome these limitations, recent research has gradually shifted its focus toward distributed cooperative control frameworks.

During the development of distributed cooperative control, multi-agent reinforcement learning (MARL)-based methods have attracted increasing attention due to their adaptability in handling complex traffic interactions [7]–[9]. However, their black-box nature makes it difficult to provide rigorous stability analysis and explicit safety guarantees, which limits their applicability in safety-critical ramp-merging scenarios. To improve reliability while preserving distributed flexibility, Distributed Model Predictive Control (DMPC) has emerged as a promising alternative. By explicitly incorporating vehicle dynamics and safety constraints into a receding-horizon optimization framework, DMPC can generate real-time control actions while providing more reliable cooperative performance.

From the communication support perspective, Vehicle-to-Everything (V2X) technology based on fifth-generation New Radio (NR) offers ultra-low latency, high reliability, and high bandwidth, making it particularly suitable for scenarios requiring real-time information exchange and cooperative decision-making [10]. NR V2X Mode 2 enables direct inter-vehicle communication through the sidelink interface, where vehicles autonomously select radio resources without centralized coordination [11]. Although this distributed access mechanism improves deployment flexibility, practical communication reliability is inevitably affected by resource collisions, packet loss, and dynamic resource reselection. Nevertheless, most existing studies are still built upon ideal communication assumptions, where neighboring vehicles can continuously exchange accurate and timely trajectory information. In realistic vehicular

This work was supported in part by the National Natural Science Foundation of China under Grant No. 62671277, 62531015, and U25A20399, in part by the Basic Research Program of Jiangsu under Grant No. BK20252084, in part by the National Key Research and Development Program of China under Grant No. 2021YFA1000500(4), in part by the Shanghai Kewei under Grant No. 24DP1500500, and in part by the Hong Kong Research Grant Council under the Areas of Excellence (AoE) Scheme Grant No. AoE/E-601/22-R. (Corresponding author: Qiong Wu.)

Qianju Shen and Qiong Wu are with the School of Automation and Intelligent Science (School of IoT), Jiangnan University, Wuxi 214122, China (e-mail: qianjushen@stu.jiangnan.edu.cn; qiongwu@jiangnan.edu.cn).

Pingyi Fan is with the Department of Electronic Engineering, State Key laboratory of Space Network and Communications, Beijing National Research Center for Information Science and Technology, Tsinghua University, Beijing 100084, China (e-mail: fpy@tsinghua.edu.cn).

Kezhi Wang is with the Department of Computer Science, Brunel University, London, Middlesex UB8 3PH, U.K. (e-mail: Kezhi.Wang@brunel.ac.uk).

Wen Chen is with the Department of Electronic Engineering, Shanghai Jiao Tong University, Shanghai 200240, China (e-mail: wenchen@sjtu.edu.cn).

Cui Zhang is with the School of Internet of Things Engineering, Wuxi Institute of Technology, Wuxi, 214121, China (e-mail: zhangcui@wxit.edu.cn).

Guoqiang Mao is with the School of Transportation, Southeast University, Nanjing 210096, China (e-mail: g.mao@ieee.org).

Khaled B. Letaief is with the Department of Electrical and Computer Engineering, the Hong Kong University of Science and Technology, Hong Kong (e-mail: eekhaled@ust.hk).

Copyright 'For the purpose of open access, the author has applied a 'Creative Commons Attribution (CC BY) licence to any Author Accepted Manuscript version arising.'

networks with dynamic and complex environments, such assumptions are often difficult to satisfy [12]–[15].

Several recent studies have begun to investigate the impact of communication conditions on cooperative vehicle control performance [16]. However, existing analytical frameworks still exhibit limitations in the cross-layer integration of communication modeling and control design. On the one hand, lower-layer communication modeling has not fully kept pace with the evolution of modern communication standards. Many existing models are still based on conventional LTE-V2X protocols and fail to capture the new resource allocation mechanisms introduced by 5G NR V2X, especially the significant influence of the resource re-evaluation mechanism on the dynamic evolution of channel states [17]. On the other hand, the control layer often responds to communication uncertainty in a passive manner [18]. Existing approaches typically model communication impairments, such as packet loss and delay, into bounded external disturbances and rely solely on controller feedback for compensation, lacking deep coupling between communication-state prediction and control decision-making. Consequently, under complex and non-ideal communication environments, existing systems often struggle to simultaneously ensure high-efficiency cooperation and safe multi-vehicle operation.

This paper addresses the gap between communication uncertainty and cooperative control in ramp-merging scenarios by proposing a communication-aware distributed model predictive control (CA-DMPC) framework, which integrates NR V2X communication performance with distributed vehicle control[1]. Unlike existing works that either assume ideal communication or treat communication uncertainty as simple stochastic disturbances, this paper explicitly models the communication dynamics and systematically integrates their impact into the control framework, which enhances the constraints of the physical boundaries. The main contributions of this work are summarized as follows:

1) We develop a novel communication-aware distributed control framework for cooperative ramp merging, in which the NR V2X Mode 2 resource re-evaluation mechanism is explicitly incorporated into the vehicle coordination process. Unlike existing ramp-merging controllers that assume ideal communication, the proposed framework captures practical sidelink resource conflicts, packet collisions, and dynamic reselection behaviors during cooperative decision-making.
2) We establish a systematic communication to control uncertainty mapping method that transforms stochastic communication impairments, including delay, packet loss, and channel collisions, into spatial prediction errors. Based on the predicted communication states, an adaptive safety margin mechanism is designed and embedded into the MPC constraints to enhance safety and recursive feasibility under unreliable communication.
3) To enable real-time distributed implementation, we decompose the original communication-control coupled optimization problem into two tractable subproblems under a block coordinate descent framework. In particular, the nonconvex control subproblem is sequentially convexified and reformulated as a quadratic programming (QP) problem, which can be efficiently solved online with significantly reduced computational complexity while preserving robust merging performance.

[1]The source code is available at: https://github.com/qiongwu86/Communication-Aware-Distributed-Control-for-Cooperative-Ramp-Merging-in-Vehicluar-Networks

The structure of this paper is organized as follows: Section II discusses the related work. Section III introduces the system model. Section IV analyzes NR V2X resource reservation based on a Markov chain. Section V presents the CA-DMPC framework for addressing multi-vehicle control problems. Section VI formulates the overall optimization problem and further decouples it into two tractable subproblems. Section VII presents the simulation results. Finally, Section VIII concludes the paper with a summary of the main findings.

II. Related work

A. V2X Communication Modeling

Existing studies have extensively examined the Semi-Persistent Scheduling (SPS) mechanism in C-V2X [19]. Gu *et al.* [20] proposed a Coordinated Resource Reservation (CRR) protocol based on an enhanced SPS scheme for vehicular resource scheduling. By coordinating error detection among vehicles within a platoon, the protocol improves resource reservation and effectively reduces collisions and latency. N.B.A. *et al.* [21] developed a multidimensional Discrete-Time Markov Chain (DTMC) model to analyze and compare the Medium Access Control (MAC) layer performance of IEEE 802.11p and C-V2X Mode 4. Furthermore, Gu *et al.* [22] introduced an analytical SPS model to quantify the impact of beacon transmission rate and resource configuration on access collision probability and latency outage. This model provides an important theoretical foundation for optimizing communication parameters such as signal detection range, transmission power, and resource reservation strategies.

In addition, several studies have focused on NR V2X. In [23], Lucas *et al.* proposed an analytical model that considers different numerologies, as well as various modulation and coding schemes, to estimate 5G latency at the wireless network layer. Todisco *et al.* [24] introduced a standards-compliant dual initial transmission resource allocation mechanism, which more effectively utilizes the resource re-evaluation mechanism in NR V2X. In [25], Cao *et al.* proposed an Improved Random Selection (IRS) scheme to reduce resource collision probability and further introduced a Deep Deterministic Policy Gradient (DDPG)-based algorithm to overcome the limitations of inter-platoon cooperation relying solely on local information. Despite these important advances, prior studies mainly focus on protocol enhancement or communication performance evaluation, while the resource re-evaluation mechanism in NR V2X Mode 2 remains insufficiently characterized in existing analytical studies.

B. Cooperative Vehicle Control for Ramp Merging

Cooperative control for ramp-merging scenarios has been widely studied in recent years. A large portion of the early

literature adopted centralized coordination frameworks, where an infrastructure unit gathers traffic information and computes globally coordinated actions for all participating vehicles. In [26], Chen *et al.* cast the merging process as a joint sequencing and trajectory optimization problem using mixed-integer nonlinear programming, enabling coordinated management of ramp and mainline traffic flows. Rios-Torres *et al.* [27] established an energy-efficient optimal control framework with explicit safety constraints for vehicles operating in the merging zone. In [28], Hou *et al.* introduced a hierarchical coordination strategy, where the upper layer determines the desired merging order and the lower layer tracks the assigned maneuvers. Although centralized methods can exploit global traffic information, their reliance on infrastructure support and centralized computation limits scalability in large or dense traffic networks.

To improve scalability and reduce infrastructure dependence, distributed control approaches have also been investigated. Zhou *et al.* [29] proposed a distributed rule-based method, where ramp vehicles identify admissible gaps in the mainline flow and negotiate merging opportunities based on local traffic observations. In [30], Hwang *et al.* presented a behavior-management framework based on a finite-state machine, allowing vehicles to switch among different driving modes according to surrounding traffic situations. Xue *et al.* [31] proposed a hierarchical distributed optimization strategy, where one layer determines feasible insertion locations and another layer coordinates vehicle motions through speed and spacing regulation. Compared with centralized schemes, distributed approaches offer better flexibility and scalability, but their coordination quality depends strongly on local information consistency.

Recently, learning-based methods have emerged as an alternative solution for cooperative ramp merging [32]. In [33], Chen *et al.* developed a MARL approach for mixed traffic environments, where multiple agents learn cooperative merging behaviors through interaction with surrounding vehicles. In [34], Hu *et al.* further introduced a cooperative multi-agent decision-making framework augmented with large language models. By integrating scene understanding, hierarchical planning, agent communication, and reflective reinforcement learning, their approach achieves efficient and safe coordination in multi-lane ramp-merging scenarios. These learning-based approaches are attractive for handling complex nonlinear dynamics and uncertain environments [35]–[37], but their black-box nature makes it challenging to provide rigorous stability analysis and explicit safety guarantees.

C. Cooperative Control under Imperfect Communication

While the aforementioned control strategies have significantly advanced vehicle coordination, they generally assume perfect communication and do not incorporate network uncertainty into the control framework. In parallel, a number of works have explored V2X-based cooperative vehicle control. Tong *et al.* [38] examined latency and packet-loss characteristics in V2V communication and proposed a channel-performance metric specifically designed for ramp-merging environments. They also introduced an Exponentially Weighted Average Age of Information metric and developed a reinforcement-learning-based merging controller capable of adapting to varying communication performance. Fang *et al.* [39] first formulated an optimal-control model for autonomous ramp merging under ideal conditions, and subsequently analyzed the statistical properties of V2I communication. They proposed a statistical delay-estimation model, and the corrected vehicle states were then used to compute the corresponding control law. Zhang *et al.* [40] combined the multiple shooting method with MPC to design a hybrid MPC framework that generates optimal reference speed trajectories for the high-level controller, a car-following model was then established, where the predictive controller tracks the reference speed and computes optimal acceleration while ensuring safety constraints. In [41], Li *et al.* investigated edge-assisted V2X motion planning under channel uncertainty and proposed a joint motion planning and power control framework that explicitly accounts for communication delays to improve driving safety. Despite these advances, existing studies typically model communication uncertainty through simplified delay or packet-loss abstractions, while proactive control design based on the predicted NR V2X Mode 2 communication-state evolution remains largely unexplored.

Different from these studies, this work links NR V2X Mode 2 resource re-evaluation to distributed MPC by using a Markov model to predict communication states, converting these predictions into spatial uncertainty, and incorporating this uncertainty into MPC safety constraints through an adaptive margin.

III. System Model

A. Ramp Merging Scenario

The ramp-merging scenario and the overall system framework considered in this study are depicted in Fig. 1. The scenario consists of two roadway types, the main road and the on-ramp. As vehicles enter the merging zone, they encounter pronounced speed differentials, fluctuating inter-vehicle gaps, and potential conflict points, making efficient and safe cooperative merging within a limited spatial region crucial. To meet this requirement, we employ a distributed control architecture in which each vehicle autonomously determines its actions based on its own state and the information exchanged with nearby vehicles.

Each vehicle is equipped with V2X communication capability and periodically broadcasts its local state information, including position, velocity, acceleration, and predicted motion trajectory. Based on the received information from neighboring vehicles, each vehicle constructs a local traffic view and performs distributed decision-making without relying on centralized infrastructure support.

At each control step, each vehicle computes its control input by solving a local optimization problem subject to vehicle-dynamics constraints and collision-avoidance requirements. The overall control objective is to achieve smooth, safe, and efficient merging for all vehicles while maintaining traffic stability and driving comfort.

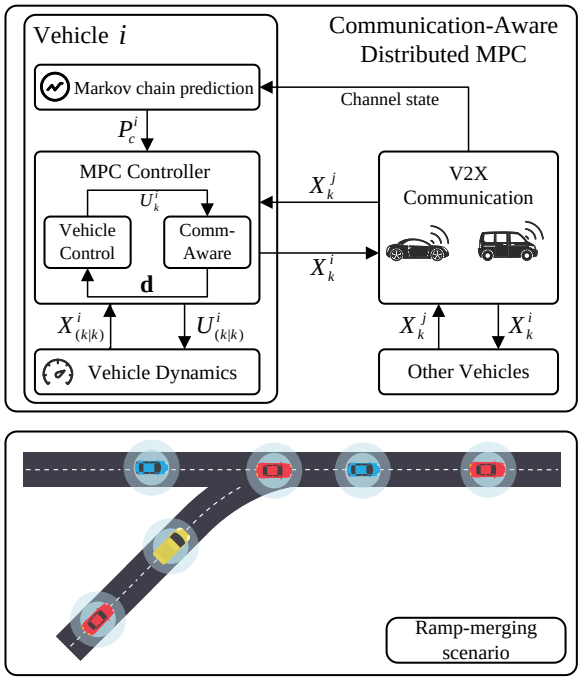

Fig. 1. Ramp-merging scenarios and CA-DMPC framework

Since communication links may suffer from packet collisions, transmission delays, and temporary outages, the received neighboring information may be outdated or incomplete. Therefore, communication uncertainty must be explicitly considered in the cooperative control framework, which motivates the communication-aware modeling developed in the following sections.

B. Resource Allocation in 5G NR V2X Mode 2

This work considers NR V2X Mode 2 sidelink communication, where vehicles autonomously select transmission resources without centralized scheduling. Such a distributed access mode is well suited to ramp-merging scenarios, in which infrastructure support may be unavailable or limited.

In NR V2X Mode 2, vehicles within the same geographical region share a resource pool organized as a two-dimensional time-frequency grid [42]. In the time domain, resources are divided into slots whose duration depends on the numerology index μ. In the frequency domain, multiple consecutive resource blocks (RBs) form a subchannel, which is the smallest unit of resource allocation. Each resource pool adopts a single numerology configuration and a fixed subchannel size.

In NR V2X Mode 2, broadcast communication adopts an enhanced distributed scheduling mechanism known as SPS. Upon the generation of a new data packet, the vehicle initiates a sensing procedure over a predefined sensing window. Within this window, the vehicle collects the received SCI, Reference Signal Received Power (RSRP), and channel busy indicators to evaluate the occupancy of candidate subchannels. A candidate resource list is then generated based on the sensing results.

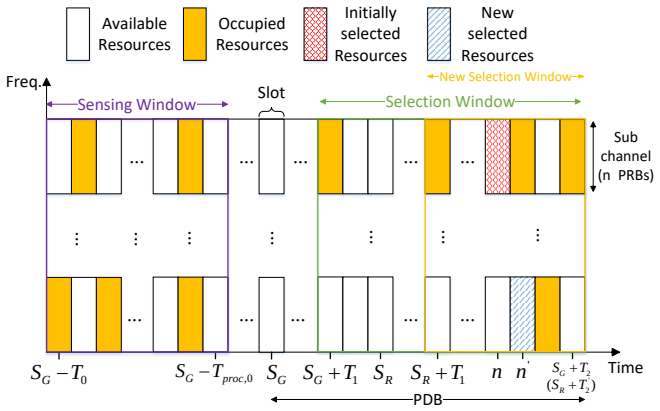

Fig. 2. NR V2X resource selection and re-evaluation

After sensing is completed, the vehicle defines a selection window. Within this window, it randomly selects one available resource and reserves it for repeated transmissions over an SPS period. The reservation remains active until the Re-selection Counter (RC) reaches zero.

The re-selection counter determines the number of consecutive packet transmissions within an SPS period. Each time the vehicle transmits a packet using its reserved resource, the RC decreases by one. When the RC reaches zero, the vehicle initiates a new sensing and resource selection procedure, and the RC is reinitialized with a random value. At the beginning of each new SPS period, the vehicle adopts one of two resource selection strategies according to the resource keeping probability p_0. With probability $1 - p_0$, it selects a new available resource from the selection window; with probability p_0, it retains the resource used in the previous SPS period.

In highly dynamic traffic environments, however, vehicle mobility and topology changes may cause previously selected resources to become suboptimal or collision-prone. To address this issue, NR V2X introduces a resource re-evaluation mechanism. Before the reserved transmission instant, the vehicle performs an additional sensing check to determine whether the currently reserved resource remains available. If the resource is found to be occupied or unreliable, a new candidate resource is selected within an updated selection window.

As illustrated in Fig. 2, S_G denotes the packet generation time. The sensing window ends at $S_G - T_{\text{proc},0}$, where $T_{\text{proc},0}$ denotes the processing interval required for the sensing information to become available for resource selection. Suppose a vehicle initially selects a transmission resource at slot n. It then performs a resource sensing operation at slot $S_R = n - T_3$ to determine whether the resource at slot n remains valid or has been excluded. According to 3GPP NR V2X specifications, the time gap T_3 is set to $T_{\text{proc},1}$, which represents the physical-layer processing time associated with resource selection or reselection. Unlike $T_{\text{proc},0}$, which determines the end of the sensing window, $T_{\text{proc},1}$ is used here to specify the processing-time offset before the reserved transmission. This operation performed at slot S_R is referred to as the re-evaluation check.

The outcome of the re-evaluation check determines whether a resource replacement needs to be triggered [43]. If the

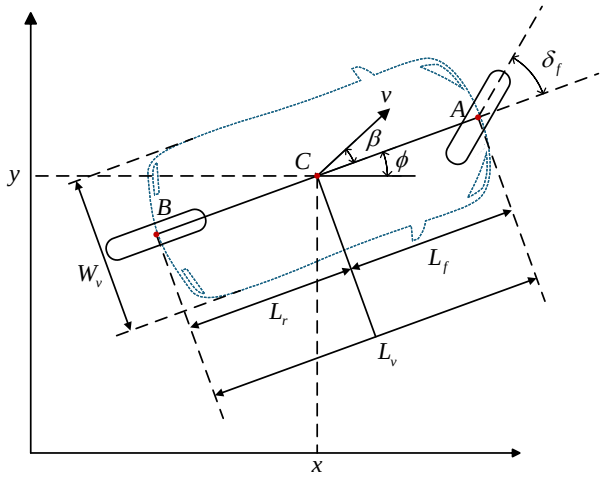

Fig. 3. Vehicular kinematic model

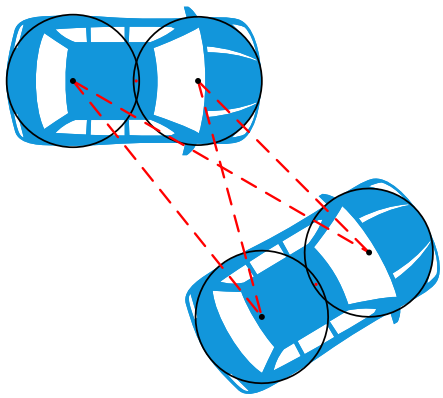

Fig. 4. Dual-circle vehicle approximation model

originally selected resource at slot n is found to be occupied or invalid, the vehicle selects a new resource within an updated selection window SW', defined as $[S_R + T_1, S_R + T_2']$ where T_2' satisfies $T_{2,min} \leq T_2' \leq PDB - (S_R - S_G)$, ensuring that the upper bound of the new selection window does not violate the Packet Delay Budget (PDB) of the corresponding Transport Block (TB).

The re-evaluation mechanism significantly affects future transmission reliability, since it changes the probability of successful reservation, collision occurrence, and subsequent resource evolution. Therefore, explicitly modeling this mechanism is essential for accurately characterizing communication-state transitions in cooperative vehicular networks.

C. Vehicle Kinematic Model

In this study, a kinematic bicycle model is adopted to describe the planar motion of each vehicle. As illustrated in Fig. 3, this model maintains a low computational complexity while effectively capturing the coupling characteristics between the longitudinal and lateral dynamics, thereby providing a reliable dynamic foundation for the subsequent control and optimization algorithm design. The vehicle motion is described by the state vector $X = [x, y, \phi, v]^T$ and the control input $U = [a, \delta_f]^T$, with system function f_c given by

$$\dot{X} = f_c(X, U) = \begin{bmatrix} v\cos(\phi + \beta) \\ v\sin(\phi + \beta) \\ \dfrac{v\sin(\beta)}{L/2} \\ a \end{bmatrix}. \tag{1}$$

In the kinematic model, the left and right wheels of the vehicle are simplified into a single equivalent wheel. The steering angle of the front wheel is denoted by δ_f. Points A and B represent the front and rear ends of the vehicle, while point C denotes the vehicle's center of mass. The distances from point C to points A and B are denoted as L_f and L_r, respectively, hence, the total vehicle length is $L = L_f + L_r$. The angle between the vehicle's longitudinal axis and the global x-axis is the yaw angle, denoted by ϕ. The vehicle's longitudinal acceleration is represented by a. The vehicle's sideslip angle β is defined as:

$$\beta = \arctan\left(\frac{L_r}{L_r + L_f}\tan\delta_f\right). \tag{2}$$

Using the forward Euler method with sampling interval Δt, the continuous vehicle dynamics are discretized as

$$X_{k+1}^i = f_d(X_k^i, U_k^i) = X_k^i + \Delta t\, f_c(X_k^i, U_k^i), \tag{3}$$

where X_k^i and U_k^i denote the state and control input of vehicle i at time $k\Delta t$, respectively.

As illustrated in Fig. 4, the dual-circle vehicle approximation model is employed to efficiently represent vehicle geometry and construct collision-avoidance constraints within a numerical optimization framework. Each vehicle is approximated by two circles of equal radius that represent its front and rear sections. The centers of these circles are aligned along the vehicle's longitudinal symmetry axis and are located at a distance l_c from the geometric center, where $l_c = \frac{1}{2}(L_v - W_v)$. An index $p \in \{1, -1\}$ is introduced to indicate the position of each circle center, with $p = 1$ denoting the front circle and $p = -1$ denoting the rear circle. To prevent collisions between any two vehicles i and j, the Euclidean distance between every pair of circle centers from both vehicles is required to exceed the sum of their safety radii. Accordingly, the relative position vector between the circle centers of vehicles is defined as:

$$\begin{aligned} &d(X^i, X^j, p, q) \\ &= \begin{bmatrix} x_i - x_j + l_c(p\cos\phi_i - q\cos\phi_j) \\ y_i - y_j + l_c(p\sin\phi_i - q\sin\phi_j) \end{bmatrix}, p, q \in \{1, -1\}, \end{aligned} \tag{4}$$

For compact representation within the optimization problem, the distances between the four pairs of circle centers are collected into the vector $D(X^i, X^j)$, expressed as:

$$D(X^i, X^j) = \begin{bmatrix} \|d(X^i, X^j, 1, 1)\|_2 \\ \|d(X^i, X^j, 1, -1)\|_2 \\ \|d(X^i, X^j, -1, 1)\|_2 \\ \|d(X^i, X^j, -1, -1)\|_2 \end{bmatrix}. \tag{5}$$

TABLE I
IMPORTANT SYMBOLS

Symbol	Description
i, j	Indices of vehicles.
k	Current discrete control step.
n	Prediction-step index within the MPC horizon.
Δt	Control sampling interval.
T_{pred}	Prediction horizon of MPC.
X_k^i	State vector of vehicle i at time step k.
$\bar{\mathbf{X}}_k^i$	Reference trajectory of vehicle i.
U_k^i	Control input vector of vehicle i.
$\bar{\mathbf{X}}_k^i$	Nominal trajectory of vehicle i over the prediction horizon.
d_{comm}	Communication-aware adaptive safety margin.
D_s	Baseline safety distance.
$D(X^i, X^j)$	Vector of distances between the four pairs of circle centers of vehicles i and j.
$\varepsilon^i_{(k+n\|k)}$	Spatial prediction error of vehicle i at prediction step $(k+n\|k)$.
$\varepsilon_{\text{base}}$	Baseline spatial prediction error under successful packet reception.
$\Delta\varepsilon_i$	One-step increment of stale-information-induced spatial error.
$\boldsymbol{\pi}^i_{(k)}$	Communication-state probability vector of vehicle i at step k.
$\mathbf{P}$	Markov state transition matrix.
$\mathbf{P}_{CC}, \mathbf{P}_{CT}, \mathbf{P}_{TC}, \mathbf{P}_{TT}$	Submatrices of the Markov transition matrix.
p, q	Lower and upper bounds of the reselection counter states.
p_0	Resource keeping probability.
p_c	Resource collision probability in NR V2X Mode 2.
P_f^{proc}	Failure probability caused by insufficient re-evaluation processing time.
P_f^{col}	Collision probability caused by resource reselection overlap.
$E[O]$	Expected overlap length of two resource selection windows.
S_G	Packet generation time.
S_R	Resource re-evaluation check time.
T_1	Lower time offset of the NR V2X resource selection window.
T_2	Upper time offset of the NR V2X resource selection window.
T_3	Time offset before the reserved transmission resource for triggering re-evaluation.
$T_{\text{proc},0}$	Processing time required for sensing.
$T_{\text{proc},1}$	Processing time required for resource selection or reselection.
$\boldsymbol{\Xi}_k^{i,j}$	Stacked safety-constraint violation vector between vehicles i and j.

IV. MARKOV MODELING OF NR V2X RESOURCE RESERVATION AND RE-EVALUATION

A. Collision Probability Analysis Considering Re-evaluation

We develop a Markov chain based analytical model to evaluate network performance in NR V2X. In the C-V2X resource selection mechanism, once a vehicle selects a resource that conflicts with those chosen by other vehicles, the resource will continue to be retained over multiple subsequent transmission periods, thereby repeatedly triggering collisions. According to the analysis in [22], the access collision probability of vehicle X_i, denoted as P_{ac}, can be obtained. This probability reflects the persistent collision risk that arises when a vehicle selects a conflicting resource in the absence of a re-evaluation mechanism. In contrast, NR V2X introduces a resource re-evaluation mechanism that allows vehicles to recheck the initially selected resources and promptly replace them when potential conflicts are detected, thereby reducing the probability of access collisions. However, despite its intended robustness enhancement, the re-evaluation mechanism may still fail under certain circumstances. In the following analysis, we investigate the failure probability of the re-evaluation mechanism and examine its impact on the overall resource collision probability.

The first failure mode is processing-time failure. According to the 3GPP specification [44], re-evaluation can be triggered when the pre-selected transmission resource lies within the nominal time window $[S_G + T_1,\ S_G + T_2]$. However, the re-evaluation operation requires a processing time of $T_3 = T_{\text{proc},1}$. Therefore, if the selected resource is located within $[S_G + T_1,\ S_G + T_3]$, the remaining time is insufficient to complete sensing and reselection before transmission. As a result, the effective re-evaluation region is reduced to $[S_G + T_3,\ S_G + T_2]$, while resources falling into $[S_G + T_1,\ S_G + T_3]$ cannot be re-evaluated. Let P_f^{proc} denote the probability of this processing-time failure, which is given by

$$P_f^{proc} = \frac{T_3 - T_1}{W}. \tag{6}$$

In Eq. (6), W represents the total length of the resource selection window, which equals $T_2 - T_1$. Second, the mechanism also fails if the re-selection following a re-evaluation still results in a collision. Specifically, after a resource collision has occurred between two vehicles, the ego vehicle's re-evaluation mechanism can detect this conflict and trigger a resource re-selection process. However, in high density environments, the newly selected resource still has a high probability of overlapping with the resources of other vehicles. To further analyze this issue, we first calculate the probability of selection window overlap between the ego vehicle and an interfering vehicle. Assume the interfering vehicle's resource selection window length is W, ego vehicle's new resource selection window, executed after the re-evaluation is triggered, is typically shorter and denoted as W_{re}, which is defined as $W_{\text{re}} = T_2' - T_1$.

To further quantify the overlap between two selection windows, the probability that the two windows overlap can be expressed as:

$$P_O = 1 - \frac{(RRI - W - W_{re} + 1)(RRI - W - W_{re} + 2)}{(RRI - W + 1)(RRI - W_{re} + 1)}, \tag{7}$$

in the expression, we assume that $RRI > W + W_{re}$. Based on this, we aim to compute the expected overlap length. Since the overlap length is a discrete positive integer and the maximum

overlap length does not exceed W_{re}, the tail-sum formula can be applied to calculate the expected overlap length [45]:

$$E[O] = \sum_{m=1}^{W_{re}} \Pr(O \geq m) = \sum_{m=1}^{W_{re}} [1 - \Pr(O \leq m-1)], \quad (8)$$

m denotes the integer threshold of the overlap length. Instead of computing $\Pr(O \geq m)$ directly, we derive its complementary event by evaluating the number of window combinations that yield an overlap of at most $m-1$. By mathematically simplifying the sum of all these non-overlapping and partially overlapping configurations, the expected overlap length can be expressed as:

$$E[O] = \sum_{m=1}^{W_{re}} \left[1 - \frac{(N_{gap} + m - 1)(N_{gap} + m)}{(RRI - W + 1)(RRI - W_{re} + 1)}\right], \quad (9)$$

where $N_{gap} = RRI - W - W_{re} + 1$. Given this expected overlap length $E[O]$, we can formulate the probability of a resource selection collision during the re-evaluation phase, denoted as P_f^{col}. This requires both vehicles to select resources from the shared overlapping region:

$$P_f^{col} = P_O \cdot \underbrace{\frac{(N_{sc}E[O])^2}{N_a N_{ra}}}_{P_{Sh|O}} \cdot \frac{N_{sc}E[O] - C_{ex}}{N_{cs}N_{rcs}}. \quad (10)$$

Here, $P_{Sh|O}$ represents the conditional probability of selecting shared resources given an overlap. The system parameters are defined as follows: N_{sc} is the number of subchannels per slot; N_a and N_{ra} are the total available resources in the windows of the ego and interfering vehicles, respectively; N_{cs} and N_{rcs} denote the sizes of their candidate resource sets; and C_{ex} represents the number of resources jointly excluded by both vehicles [46].

Based on the above derivations, we can obtain the collision probability in the NR V2X resource selection mechanism with the re-evaluation procedure as follows:

$$p_c = P_{ac}(P_f^{proc} + (1 - P_f^{proc})P_f^{col}). \quad (11)$$

The derived collision probability p_c explicitly captures the impact of the re-evaluation mechanism and is subsequently used to construct the communication-state transition model for predictive control design.

B. Markov Transition Matrix Construction

To characterize the evolution of resource reservation outcomes, a finite-state Markov chain is constructed, as shown in Fig. 5. Two classes of states are considered:

1) C_k: collision states, where the vehicle remains on a colliding reserved resource with RC stage k;
2) T_k: successful transmission states, where the reserved resource is collision-free with RC stage k.

Here, $k \in \{1, \ldots, q\}$ denotes the remaining re-selection counter stage, and p and q are the lower and upper initialization bounds of the RC.

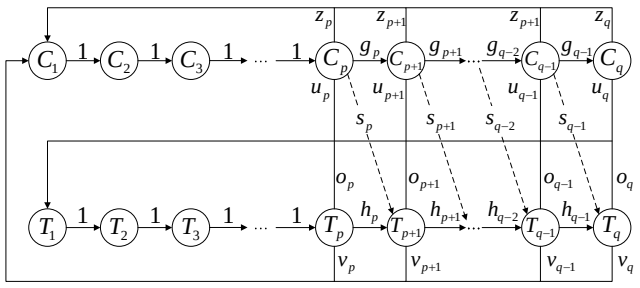

Fig. 5. Markov chain-based analytical model

Based on the defined communication states and the corresponding SPS reservation dynamics, the overall state transition matrix is written as

$$P = \begin{bmatrix} P_{CC} & P_{CT} \\ P_{TC} & P_{TT} \end{bmatrix}, \quad (12)$$

where the four submatrices characterize transitions between collision and successful transmission states. The matrix dimension is $2q \times 2q$, and each submatrix is derived according to the reservation persistence, reselection, and collision-resolution behaviors of the SPS mechanism.

The probability of transitioning from C_k to C_{k+1} is:

$$P_{k,k+1} = \begin{cases} 1, & 1 \leq k < p, \\ g_k, & p \leq k < q. \end{cases} \quad (13)$$

For $1 \leq k < p$, as the resource reservation collision persists, the vehicle stays in the collision state until the RC counter reaches zero, hence, the transition probability equals 1. For $p \leq k < q$, the transitioning probability from C_k to C_{k+1} is g_k, defined as:

$$g_k = \frac{(q-k)^2}{(q-k+1)^2} + p_0 \frac{(q-k)}{(q-k+1)^2}. \quad (14)$$

This probability consists of two components: The first term, $\frac{(q-k)^2}{(q-k+1)^2}$, represents the probability that both the ego and interfering vehicles have RC counters greater than zero; The second term, $p_0 \frac{(q-k)}{(q-k+1)^2}$, corresponds to the case where the interfering vehicle's RC counter has reached zero but continues to occupy the same resource due to the resource-holding probability p_0.

The probability of transitioning from C_k to C_1 is given by:

$$P_{k,1} = \begin{cases} 0, & 1 \leq k < p, \\ z_k, & p \leq k \leq q, \end{cases} \quad (15)$$
$$z_k = w_k + r_k p_c.$$

In Eq. (15), w_k represents two cases: (i) both vehicles' RC counters reach zero and each retains its resource with probability p_0, or (ii) the interfering vehicle still has a nonzero RC counter while the ego vehicle retains its resource with probability p_0. It is computed as:

$$w_k = \frac{p_0^2}{(q-k+1)^2} + p_0 \frac{(q-k)}{(q-k+1)^2}. \quad (16)$$

The second term, $r_k p_c$, accounts for the case where the ego vehicle reselects its resource but still experiences a collision with probability p_c, where:

$$r_k = \frac{1-p_0}{q-k+1}. \tag{17}$$

Thus, the sub-matrix P_{CC} can be represented as:

$$P_{CC} = \begin{bmatrix} 0 & 1 & 0 & \cdots & 0 & 0 \\ \vdots & \vdots & \ddots & & \vdots & \vdots \\ z_p & 0 & \cdots & g_p & \cdots & 0 \\ \vdots & \vdots & & & \ddots & 0 \\ z_{q-1} & 0 & 0 & \cdots & 0 & g_{q-1} \\ z_q & 0 & 0 & \cdots & 0 & 0 \end{bmatrix}. \tag{18}$$

The probability of transitioning from C_k to T_1 is given by:

$$\begin{aligned} P_{k,q+1} &= \begin{cases} 0, & 1 \le k < p, \\ u_k, & p \le k \le q, \end{cases} \\ u_k &= \frac{p_0(1-p_0)}{(q-k+1)^2} + r_k(1-p_c). \end{aligned} \tag{19}$$

In Eq. (19), the first term represents the case where the ego vehicle continues to use its current resource while the interfering vehicle reselects another resource, thereby resolving the collision. The second term corresponds to the scenario where the ego vehicle reselects a new resource and successfully avoids collision.

The probability of transitioning from C_k to T_{k+1} is:

$$\begin{aligned} P_{k,q+k+1} &= \begin{cases} 0, & 1 \le k < p, \\ s_k, & p \le k < q, \end{cases} \\ s_k &= \frac{(1-p_0)(q-k)}{(q-k+1)^2}, \end{aligned} \tag{20}$$

In Eq. (20), s_k represents the case where the interfering vehicle reselects another resource, while the ego vehicle continues using its current one. Therefore, the sub-matrix P_{CT} can be written as:

$$P_{CT} = \begin{bmatrix} 0 & \cdots & 0 & \cdots & 0 \\ \vdots & \ddots & \vdots & & \\ u_p & \cdots & s_p & 0 & \vdots \\ \vdots & & & \ddots & \\ u_{q-1} & 0 & \cdots & \cdots & s_{q-1} \\ u_q & 0 & \cdots & \cdots & 0 \end{bmatrix}. \tag{21}$$

If the ego vehicle reselects resources and collides with another vehicle, it moves from the transmission state to the collision state, the transition probability is v_k, which equals $r_k p_c$. Accordingly, the sub-matrix P_{TC} is expressed as:

$$P_{TC} = \begin{bmatrix} 0 & 0 & \cdots & 0 \\ \vdots & \vdots & & \vdots \\ v_p & 0 & \cdots & 0 \\ \vdots & \vdots & & \vdots \\ v_q & 0 & \cdots & 0 \end{bmatrix}. \tag{22}$$

The probability of transitioning from T_k to T_{k+1} is:

$$\begin{aligned} P_{q+k,q+k+1} &= \begin{cases} 1, & 1 \le k < p, \\ h_k, & p \le k < q, \end{cases} \\ h_k &= \frac{q-k}{q-k+1}, \end{aligned} \tag{23}$$

In Eq. (23), h_k denotes the probability that the RC counter has not yet reached zero. The transition from T_k to T_1 occurs when the RC counter reaches zero. Its probability is:

$$\begin{aligned} P_{k+q,q+1} &= \begin{cases} 0, & 1 \le k < p, \\ o_k, & p \le k \le q, \end{cases} \\ o_k &= \frac{p_0}{q-k+1} + r_k(1-p_c). \end{aligned} \tag{24}$$

In Eq. (24), the first term represents the probability that the ego vehicle retains its current resource with probability p_0, while the second term corresponds to successful reselection without collision. The sub-matrix P_{TT} can be written as:

$$P_{TT} = \begin{bmatrix} 0 & 1 & 0 & \cdots & \cdots & 0 \\ \vdots & & \ddots & & & \\ o_p & 0 & \cdots & h_p & \cdots & 0 \\ \vdots & & & & \ddots & \\ o_{q-1} & 0 & 0 & \cdots & 0 & h_{q-1} \\ o_q & 0 & \cdots & \cdots & 0 & 0 \end{bmatrix}. \tag{25}$$

The resulting transition matrix enables recursive prediction of future communication states for use in the proposed CA-DMPC framework. In this analytical model, collision-free transmissions are assumed to be successfully received. Additional decoding failures caused by small-scale fading and shadowing are not explicitly modeled. The potential impact of these effects on uncertainty prediction and possible model extensions are discussed in the conclusion.

V. Distributed collaborative MPC

A. Nominal Trajectory and Communication Uncertainty

In the MPC framework, the controller adopts a receding horizon strategy. At each control step k, vehicle i optimizes the control sequence $U^i_{(k+n|k)}$ for $n \in [0, T_{\text{pred}}-1]$ and applies only $U^i_{(k|k)}$. The corresponding predicted states $X^i_{(k+n|k)}$ for $n \in [1, T_{\text{pred}}]$ are stacked to form the nominal trajectory:

$$\bar{\mathbf{X}}^i_k = [X^{iT}_{(k+1|k)}, X^{iT}_{(k+2|k)}, \ldots, X^{iT}_{(k+T_{\text{pred}}|k)}]^T. \tag{26}$$

Vehicles exchange nominal trajectories via V2X for local MPC. When reception fails, they rely on the latest available trajectories. The Markov model predicts the distribution of communication states over the prediction horizon to quantify the resulting uncertainty.

Specifically, at time step k, given the vehicle's current observed communication state, the initial probability vector is exactly defined as a one-hot vector: $\pi^i_{k|k} = [0, \ldots, 0, 1, 0, \ldots, 0]$. Subsequently, the Markov model recursively predicts the state distribution $\pi^i_{k+n|k}$ for future prediction steps as

$$\pi^i_{(k+n|k)} = \pi^i_{(k+n-1|k)} P^i, \quad n \in [1, T_{\text{pred}}], \tag{27}$$

P is the state transition matrix obtained from Eq. (12). This recursion only involves T_{pred} matrix-vector multiplications, resulting in low computational overhead.

To address queuing delays and burst packet losses in V2X networks, we map these communication impairments into spatial prediction errors of the ego vehicle's position as estimated by its neighbors. Let the random variable $\varepsilon^i_{(k+n|k)}$ denote the spatial prediction error of vehicle i as estimated by its neighbors at prediction step $n \in [1, T_{\text{pred}}]$, given the information available at time step k. Furthermore, based on the derived Markov model, let $\pi^C_{(k+n|k)}$ and $\pi^T_{(k+n|k)}$ denote the marginal probability vectors for the collision and successful transmission states, respectively.

To characterize the impact of non-ideal communication on distributed control, a joint expected spatial error row vector $\mathbf{e}^i_{(k+n|k)} \in \mathbb{R}^{1\times 2q}$ is defined as

$$\mathbf{e}^i_{(k+n|k)} = \left[\mathbf{e}^{C,i}_{(k+n|k)}, \mathbf{e}^{T,i}_{(k+n|k)}\right], \tag{28}$$

where $\mathbf{e}^{C,i}_{(k+n|k)}$ and $\mathbf{e}^{T,i}_{(k+n|k)}$ denote the expected spatial error contributions associated with collision states and successful-transmission states, respectively.

The j-th elements of $\mathbf{e}^{C,i}_{(k+n|k)}$ and $\mathbf{e}^{T,i}_{(k+n|k)}$ are defined according to the law of total expectation as

$$e^{C,i}_{j,(k+n|k)} = \mathbb{E}\big[\varepsilon^i_{(k+n|k)} \mid C^i_j\big] \cdot \pi^{C,i}_{j,(k+n|k)}, \quad j \in \{1,\dots,q\} \tag{29}$$

$$e^{T,i}_{j,(k+n|k)} = \mathbb{E}\big[\varepsilon^i_{(k+n|k)} \mid T^i_j\big] \cdot \pi^{T,i}_{j,(k+n|k)}, \quad j \in \{1,\dots,q\} \tag{30}$$

where $\pi^{C,i}_{j,(k+n|k)}$ and $\pi^{T,i}_{j,(k+n|k)}$ are the corresponding state probabilities. When the newest packet is successfully received, the accumulated uncertainty is reset, and only a baseline uncertainty remains. This baseline term, denoted by $\varepsilon^i_{\text{base}}$, captures the residual error under successfully refreshed communication, including modeling imperfections and the effect of small communication delay.

If packet reception fails due to collision or communication outage, neighboring vehicles must continue predicting the motion of vehicle i using outdated trajectory information. In this case, the uncertainty increases by a one-step increment

$$\Delta\varepsilon^i = v^{\max}_i \Delta t + \frac{1}{2} a^{\max}_i (\Delta t)^2, \tag{31}$$

where Δt is the control sampling interval, and $v^{\max}_i$ and $a^{\max}_i$ are the maximum velocity and acceleration bounds of vehicle i, respectively.

Within the prediction horizon $n \in [1, T_{\text{pred}}]$, the expected spatial uncertainty evolves according to the Markov transition submatrices P^i_{CC}, P^i_{TC}, P^i_{CT}, and P^i_{TT}.

If the communication state of vehicle i transitions to a successful-transmission state, a fresh trajectory update is received and the accumulated stale-information error is cleared. In this case, the conditional expected uncertainty under any successful-transmission state is approximated by the same baseline term $\varepsilon^i_{\text{base}}$. Therefore,

$$\begin{aligned}\mathbf{e}^{T,i}_{(k+n|k)} &= \pi^{T,i}_{(k+n|k)} \varepsilon^i_{\text{base}} \\ &= \left(\pi^{C,i}_{(k+n-1|k)} P^i_{CT} + \pi^{T,i}_{(k+n-1|k)} P^i_{TT}\right) \varepsilon^i_{\text{base}}.\end{aligned} \tag{32}$$

If the communication state of vehicle i falls into a collision state, no fresh packet is received. In this case, the baseline uncertainty has already been inherited from the previous step, and only the additional one-step stale-information increment needs to be accumulated. Hence, the expected uncertainty under collision states is recursively updated as

$$\begin{aligned}\mathbf{e}^{C,i}_{(k+n|k)} = &\underbrace{\left(\mathbf{e}^{C,i}_{(k+n-1|k)} + \pi^{C,i}_{(k+n-1|k)} \cdot \Delta\varepsilon^i\right) P^i_{CC}}_{\text{Transition flow from } C} \\ &+ \underbrace{\left(\mathbf{e}^{T,i}_{(k+n-1|k)} + \pi^{T,i}_{(k+n-1|k)} \cdot \Delta\varepsilon^i\right) P^i_{TC}}_{\text{Transition flow from } T}\end{aligned} \tag{33}$$

At prediction step n, the expected spatial uncertainty caused by vehicle i is obtained by summing all state contributions:

$$\bar{\varepsilon}^i_{(k+n|k)} = \sum_{j=1}^{q} e^{C,i}_{j,(k+n|k)} + \sum_{j=1}^{q} e^{T,i}_{j,(k+n|k)}. \tag{34}$$

To maintain numerical tractability and avoid overly conservative safety margins, the uncertainty bound is truncated by the maximum tolerable spatial error:

$$\tilde{\varepsilon}^i_{(k+n|k)} = \min\left(\bar{\varepsilon}^i_{(k+n|k)}, \varepsilon^i_{\max}\right). \tag{35}$$

B. Formulation of Communication-Aware Optimization

To reduce collision risks caused by packet drops and transmission delays, an adaptive communication-dependent safety margin, denoted by d^{comm}, is introduced into the safety-distance constraint. This margin is used to compensate for the position estimation error accumulated during communication outages. Accordingly, the following communication-aware penalty function is adopted:

$$f(d^{\text{comm}}, \tilde{\varepsilon}) = \frac{1}{1 - e^{-(d^{\text{comm}}_{(k+n|k)} - \tilde{\varepsilon}_{(k+n|k)} + \eta)/\sigma}}. \tag{36}$$

The penalty function explicitly depends on the predicted spatial uncertainty $\tilde{\varepsilon}_{(k+n|k)}$. When the optimized safety margin $d^{\text{comm}}_{(k+n|k)}$ decreases toward the uncertainty level $\tilde{\varepsilon}_{(k+n|k)}$, the denominator approaches zero and the penalty value increases rapidly. As a result, overly small safety margins are strongly discouraged during optimization.

The parameter $\eta > 0$ is a small positive constant introduced to avoid numerical singularity and maintain a positive offset in the safety margin. The parameter $\sigma > 0$ is a scaling factor that adjusts the sensitivity of the penalty function and helps balance constraint enforcement with numerical conditioning.

Based on the above discussion, the distributed MPC optimization problem is formulated as:

$$\begin{aligned}
&\min_{\substack{U^i_{(k+n|k)},\, d^{comm}_{(k+n|k)},\, i\in\mathcal{N} \\ n\in[0,T_{\text{pred}}-1]}} \\
&\sum_{i\in\mathcal{N}}\Bigg[\sum_{n=1}^{T_{\text{pred}}-1}\left\|M_f\left(X^i_{(k+n+1|k)}-X^i_{(k+n|k)}\right)\right\|^2 \\
&\quad+\sum_{n=1}^{T_{\text{pred}}}\|X^i_{(k+n|k)}-\tilde{X}^i_{(k+n|k)}\|^2_{Q_X} \\
&\quad+\sum_{n=1}^{T_{\text{pred}}}\|U^i_{(k+n-1|k)}\|^2_{Q_U} \\
&\quad+\sum_{n=1}^{T_{\text{pred}}}\frac{w_1}{1-e^{-(d^{comm,i}_{(k+n|k)}-\tilde{\varepsilon}^i_{(k+n|k)}+\eta)/\sigma}} \\
&\quad+\sum_{n=1}^{T_{\text{pred}}}w_2\big(d^{\text{comm}}_{(k+n|k)}\big)^2\Bigg] \qquad (37a)\\
\text{s.t.}\quad &\underline{U}\le U^i_{(k+n|k)}\le\overline{U}, \qquad (37b)\\
&X^i_{(k+n+1|k)}=f_d\big(X^i_{(k+n|k)},U^i_{(k+n|k)}\big), \qquad (37c)\\
&D_s+d^{\text{comm},i}_{(k+n|k)}\le D(X^i_{(k+n|k)},X^j_{(k+n|k)}), \qquad (37d)\\
&\tilde{\varepsilon}_{(k+n|k)}+\eta\le d^{comm}_{(k+n|k)}\le\bar{d}^{comm}, \qquad (37e)\\
&\forall i\in\mathcal{N},\, j\in\mathcal{N}_i.
\end{aligned}$$

The cost function consists of five components. The first term penalizes rapid variations in vehicle states, with M_f controlling the smoothness. The second term penalizes deviations between the predicted and reference trajectories, weighted by Q_X. The third term penalizes control effort via Q_U, improving driving comfort. The fourth term captures the coupling between communication uncertainty and safety margin. The fifth term encourages minimizing d^{comm} to balance safety and efficiency. Regarding the constraints, Eq. (37b) enforces actuator limitations, where $\underline{U}$ and $\overline{U}$ represent the lower and upper limits of the control inputs; Eq. (37c) represents the discrete vehicle dynamics; Eq. (37d) ensures inter-vehicle safety distances, where D_s is the baseline safety distance; and Eq. (37e) constrains the adaptive safety margin to lie within an allowable range. $\mathcal{N}_i$ denotes the neighbor set of vehicle i.

VI. Optimization problem and Solution

A. Block Coordinate Descent Framework

The control inputs U and the communication-aware safety margins d^{comm} are coupled through the collision-avoidance constraints. To solve the resulting optimization problem, a block coordinate descent (BCD) framework is adopted to decompose it into two subproblems: vehicle control optimization and safety margin optimization. These subproblems are solved alternately by fixing one variable block and optimizing the other. Each vehicle performs the optimization locally using the predicted trajectories received from its neighbors.

Fixing d^{comm} allows the vehicle control subproblem to be formulated as follows:

$$\begin{aligned}
&\min_{\substack{U^i_{(k+n|k)},\\ i\in\mathcal{N},n\in[0,T_{\text{pred}}-1]}} \\
&\sum_{i\in\mathcal{N}}\Bigg[\sum_{n=1}^{T_{\text{pred}}-1}\left\|M_f\left(X^i_{(k+n+1|k)}-X^i_{(k+n|k)}\right)\right\|^2 \\
&\quad+\sum_{n=1}^{T_{\text{pred}}}\left\|X^i_{(k+n|k)}-\tilde{X}^i_{(k+n|k)}\right\|^2_{Q_X} \\
&\quad+\sum_{n=1}^{T_{\text{pred}}}\left\|U^i_{(k+n-1|k)}\right\|^2_{Q_U}\Bigg] \qquad (38a)\\
\text{s.t.}\quad &\underline{U}\le U^i_{(k+n|k)}\le\overline{U}, \qquad (38b)\\
&X^i_{(k+n+1|k)}=f_d\left(X^i_{(k+n|k)},U^i_{(k+n|k)}\right), \qquad (38c)\\
&D_a\le D\left(X^i_{(k+n+1|k)},X^j_{(k+n+1|k)}\right), \qquad (38d)\\
&\forall i\in\mathcal{N},j\in\mathcal{N}_i.
\end{aligned}$$

In this subproblem, the objective function is a positive-definite quadratic form, and D_a in Eq. (38d) represents the sum of the communication safety distance and the basic safety distance. However, the constraints in Eq. (38c) and Eq. (38d) remain nonlinear and nonconvex, which significantly increases the computational burden and reduces solving efficiency.

To efficiently solve the non-convex vehicle-control subproblem, a Sequential Convex Programming (SCP) mechanism is embedded within the BCD framework. Instead of performing a single linearization based on the previous nominal trajectory, the proposed method iteratively updates the linearization point to better approximate the original non-convex problem.

Specifically, during each outer BCD iteration, N_{mpc} SCP inner iterations are executed. At each inner iteration, the vehicle dynamics and collision-avoidance constraints are locally linearized around the latest nominal trajectory, yielding a structured QP subproblem. After solving the QP, the obtained control sequence is forward simulated to generate an updated nominal trajectory, which is then used in the next iteration.

This iterative refinement improves the approximation accuracy of nonlinear dynamics and safety constraints while maintaining low online computational complexity. In addition, the trajectory smoothing term $||\overline{M}_f\mathbf{X}^i_k||^2$ acts as a regularization factor to suppress abrupt trajectory variations and enhance numerical stability during SCP iterations.

For compact representation, we define:

$$\begin{aligned}
\mathbf{X}^i_k&=[X^{iT}_{(k+1|k)},X^{iT}_{(k+2|k)},\cdots,X^{iT}_{(k+T_{\text{pred}}|k)}]^T,\\
\mathbf{U}^i_k&=[U^{iT}_{(k|k)},U^{iT}_{(k+1|k)},\cdots,U^{iT}_{(k+T_{\text{pred}}-1|k)}]^T.
\end{aligned} \qquad (39)$$

Here, $\mathbf{X}^i_k\in\mathbb{R}^{4T_{\text{pred}}}$ and $\mathbf{U}^i_k\in\mathbb{R}^{2T_{\text{pred}}}$ denote the stacked sequences, while X^i_k and U^i_k denote individual state and control vectors. The corresponding stacked reference trajectory is denoted by $\tilde{\mathbf{X}}^i_k$.

The continuous nonlinear vehicle dynamics are discretized via the Euler method and linearized around the nominal trajectory $(\overline{X}^i_{k+n|k},\overline{U}^i_{k+n|k})$ using a first-order Taylor expansion. This yields the following time-varying discrete affine system:

$$
\begin{aligned}
&X^i_{(k+n+1|k)} \\
&= A^i_{(k+n|k)} X^i_{(k+n|k)} + B^i_{(k+n|k)} U^i_{(k+n|k)} + G^i_{(k+n|k)},
\end{aligned} \tag{40}
$$

where $A^i_{(k+n|k)}$ and $B^i_{(k+n|k)}$ denote the discrete-time state and control matrices, respectively, derived from the Jacobians via the Euler discretization method, and $G^i_{(k+n|k)}$ represents the affine offset term.

$$
\begin{aligned}
A^i_{(k+n|k)} &= I + \Delta t J^f_X(\overline{X}^i_{(k+n|k)}, \overline{U}^i_{(k+n|k)}) \\
B^i_{(k+n|k)} &= \Delta t J^f_U(\overline{X}^i_{(k+n|k)}, \overline{U}^i_{(k+n|k)}) \\
G^i_{(k+n|k)} &= \Delta t \big[f_c(\overline{X}^i_{(k+n|k)}, \overline{U}^i_{(k+n|k)}) \\
&\quad - J^f_X(\overline{X}^i_{(k+n|k)}, \overline{U}^i_{(k+n|k)}) \overline{X}^i_{(k+n|k)} \\
&\quad - J^f_U(\overline{X}^i_{(k+n|k)}, \overline{U}^i_{(k+n|k)}) \overline{U}^i_{(k+n|k)} \big].
\end{aligned} \tag{41}
$$

Leveraging the recursive structure of the system dynamics, the stacked form of the linearized system can be expressed as:

$$
\mathbf{X}^i_k = A^i_k X^i_{(k|k)} + B^i_k \mathbf{U}^i_k + G^i_k, \tag{42}
$$

The optimization problem Eq. (38) can be formulated as:

$$
\min_{\mathbf{X}^i_k, \mathbf{U}^i_k} \quad \left\| \mathbf{X}^i_k - \tilde{\mathbf{X}}^i_k \right\|^2_{\bar{Q}_X} + \left\| \mathbf{U}^i_k \right\|^2_{\bar{Q}_U} + \left\| \bar{M}_f \mathbf{X}^i_k \right\|^2 \tag{43a}
$$

$$
\text{s.t.} \quad E^{T_{\text{pred}}} \otimes \underline{U} \le \mathbf{U}^i_k \le E^{T_{\text{pred}}} \otimes \bar{U} \tag{43b}
$$

$$
\mathbf{X}^i_k = A^i_k X^i_{(k|k)} + B^i_k \mathbf{U}^i_k + G^i_k \tag{43c}
$$

$$
E^{T_{\text{pred}}} \otimes D_a \le \mathcal{D}(\mathbf{X}^i_k, \mathbf{X}^j_k), \quad j \in \mathcal{N}_i \tag{43d}
$$

Eq. (43b) denotes the control input constraints, Eq. (43c) represents the discrete-time vehicle dynamics, and Eq. (43d) enforces the inter-vehicle safety distance constraint. The stacked distance vector

$$
\mathcal{D}(\mathbf{X}^i_k, \mathbf{X}^j_k) = \begin{bmatrix} D(X^i_{(k+1|k)}, X^j_{(k+1|k)}) \\ D(X^i_{(k+2|k)}, X^j_{(k+2|k)}) \\ \vdots \\ D(X^i_{(k+T_{\text{pred}}|k)}, X^j_{(k+T_{\text{pred}}|k)}) \end{bmatrix}, \tag{44}
$$

represents the pairwise distances between vehicles i and j across the prediction horizon T_{pred}. In the cost function, $\bar{Q}_X$ and $\bar{Q}_U$ are the block-diagonal weighting matrices for the predicted state and control input:

$$
\begin{aligned}
\bar{Q}_X &= \text{diag}(Q_X, Q_X, \ldots, Q_X, K_X Q_X), \\
\bar{Q}_U &= \text{diag}(Q_U, Q_U, \ldots, Q_U, K_U Q_U),
\end{aligned} \tag{45}
$$

K_X and K_U are terminal weights for state and control.

To suppress abrupt variations in acceleration or steering rate, a trajectory smoothing term $\bar{M}_f \mathbf{X}^i_k$ is incorporated into the cost function. The definition of $\bar{M}_f$ is given by:

$$
\bar{M}_f = \begin{bmatrix} -M_f & M_f & 0 & \cdots & 0 \\ 0 & -M_f & M_f & \cdots & 0 \\ \vdots & & \ddots & \ddots & \vdots \\ 0 & \cdots & 0 & -M_f & M_f \end{bmatrix}, \tag{46}
$$

this term penalizes the temporal difference between adjacent predicted states, thereby enforcing trajectory continuity and mitigating oscillatory control actions.

The nonlinear distance function $D(\cdot)$ in constraint Eq. (43d) makes the problem nonconvex. To approximate it in a convex form, we introduce the constraint violation function:

$$
\begin{aligned}
&\xi(X^i_{(k+n|k)}, X^j_{(k+n|k)}, p, q) \\
&= \max(0, D_a - \| d(X^i_{(k+n|k)}, X^j_{(k+n|k)}, p, q) \|),
\end{aligned} \tag{47}
$$

where $d(\cdot)$ represents the relative position vector between the geometric centers of the dual approximated circular sections. The safety constraint is satisfied if and only if $\xi = 0$.

To formulate the penalty at each prediction step, the violations for the four circle-center combinations ($p, q \in \{1, -1\}$) are concatenated into a vector $\Xi^{i,j}_{k+n|k} \in \mathbb{R}^4$. Stacking these vectors across the entire prediction horizon yields the joint constraint violation vector for vehicles i and j:

$$
\Xi^{i,j}_k = \left[(\Xi^{i,j}_{k+1|k})^T, \ldots, (\Xi^{i,j}_{k+T_{\text{pred}}|k})^T \right]^T \in \mathbb{R}^{4T_{\text{pred}}} \tag{48}
$$

Accordingly, the safety constraint is equivalently expressed as $\|\Xi^{i,j}_k\|^2 \le 0$, and the extended optimization problem is formulated as:

$$
\begin{aligned}
\min_{\mathbf{X}^i_k, \mathbf{U}^i_k} \quad & \left\| \mathbf{X}^i_k - \tilde{\mathbf{X}}^i_k \right\|^2_{\bar{Q}_X} + \left\| \mathbf{U}^i_k \right\|^2_{\bar{Q}_U} + \left\| \bar{M}_f \mathbf{X}^i_k \right\|^2 \\
& + \alpha \sum_{j \in \mathcal{N}_i} \|\Xi^{i,j}_k\|^2
\end{aligned} \tag{49a}
$$

$$
\text{s.t.} \quad E^{T_{\text{pred}}} \otimes \underline{U} \le \mathbf{U}^i_k \le E^{T_{\text{pred}}} \otimes \bar{U} \tag{49b}
$$

$$
\mathbf{X}^i_k = A^i_k X^i_{(k|k)} + B^i_k \mathbf{U}^i_k + G^i_k \tag{49c}
$$

α is a penalty coefficient that balances trajectory optimality and safety preservation.

An increase in predicted spatial uncertainty can tighten the safety constraints beyond the vehicle's actuation capability, making the optimization problem infeasible. Replacing the hard safety constraints with the quadratic penalty $\alpha \sum_{j \in \mathcal{N}_i} \|\Xi^{i,j}_k\|^2$ allows constraint violations while penalizing their magnitude.

To ensure efficient computation, the term $\Xi^{i,j}_k$ is linearized around the nominal trajectories $(\bar{\mathbf{X}}^i_k, \bar{\mathbf{X}}^j_k)$ using first-order Taylor expansion:

$$
\Xi^{i,j}_k \approx \Xi^{i,j}_k(\bar{\mathbf{X}}^i_k, \bar{\mathbf{X}}^j_k) + \frac{\partial \Xi^{i,j}_k}{\partial \mathbf{X}^i_k}\Big|_{(\bar{\mathbf{X}}^i_k, \bar{\mathbf{X}}^j_k)} (\mathbf{X}^i_k - \bar{\mathbf{X}}^i_k). \tag{50}
$$

Let us define the Jacobian matrix and the affine offset as:

$$
\begin{aligned}
K^i &= \frac{\partial \Xi^{i,j}_k}{\partial \mathbf{X}^i_k}\Big|_{(\bar{\mathbf{X}}^i_k, \bar{\mathbf{X}}^j_k)}, \\
b^i &= \Xi^{i,j}_k(\bar{\mathbf{X}}^i_k, \bar{\mathbf{X}}^j_k) - K^i \bar{\mathbf{X}}^i_k,
\end{aligned} \tag{51}
$$

the quadratic penalty term can be analytically expanded as:

$$
\begin{aligned}
\|\Xi^{i,j}_k\|^2 &\approx \|K^i \mathbf{X}^i_k + b^i\|^2 \\
&= (\mathbf{X}^i_k)^T (K^{iT} K^i) \mathbf{X}^i_k + 2(K^{iT} b^i)^T \mathbf{X}^i_k + \|b^i\|^2
\end{aligned} \tag{52}
$$

The constant term $\|b^i\|^2$ does not influence the optimal decision variables and can therefore be omitted without loss of optimality. Moreover, the matrix $(K^i)^T K^i$ is positive

semidefinite by construction, ensuring that the convexity of the objective function with respect to the state variable $\mathbf{X}_k^i$ is strictly preserved. By substituting the linearized vehicle dynamics in Eq. (43c) and the expanded penalty term in Eq. (52) into the overall objective function, and subsequently collecting terms with respect to the control input $\mathbf{U}_k^i$, the original highly coupled nonconvex problem can be reformulated as a standard convex QP.

$$\begin{aligned} \min_{\mathbf{U}_k^i} \quad & (\mathbf{U}_k^i)^T \mathcal{P} \mathbf{U}_k^i + 2\mathcal{Q}^T \mathbf{U}_k^i \\ \text{s.t.} \quad & E^{T_{\text{pred}}} \otimes \underline{U} \le \mathbf{U}_k^i \le E^{T_{\text{pred}}} \otimes \overline{U}, \end{aligned} \tag{53}$$

in the expression, $\mathcal{P}$ and $\mathcal{Q}$ are defined as follows:

$$\begin{aligned} \mathcal{P} =& B_k^{iT} \Big(\bar{Q}_X + \alpha \sum_{j \in \mathcal{N}_i} K^{iT} K^i + \bar{M}_f^T \bar{M}_f \Big) B_k^i + \bar{Q}_U, \\ \mathcal{Q} =& B_k^{iT} \Big[\alpha \sum_{j \in \mathcal{N}_i} K^{iT} b^i - \bar{Q}_X \tilde{\mathbf{X}}_k^i \\ & + \Big(\bar{Q}_X + \alpha \sum_{j \in \mathcal{N}_i} K^{iT} K^i + \bar{M}_f^T \bar{M}_f \Big) (A_k^i X_{(k|k)}^i + G_k^i) \Big]. \end{aligned} \tag{54}$$

The optimization of the communication safety margin can be solved as an independent subproblem when the control input $\mathbf{U}_k^i$ is fixed. Let

$$\mathbf{d} = [d_{k+1|k}^{\text{comm}}, \ldots, d_{k+T_{\text{pred}}|k}^{\text{comm}}]^T \in \mathbb{R}^{T_{\text{pred}}}$$

denote the sequence of communication safety margins over the prediction horizon. This subproblem is formulated as

$$\begin{aligned} \min_{\mathbf{d}} \quad & \widetilde{J}_{\text{comm}}(\mathbf{d}) = J_{\text{comm}}(\mathbf{d}) \\ & \qquad + \alpha \sum_{j \in \mathcal{N}_i} \left\| \Xi_k^{i,j} (\bar{\mathbf{X}}_k^i, \bar{\mathbf{X}}_k^j; \mathbf{d}) \right\|^2 \\ & J_{\text{comm}}(\mathbf{d}) = \sum_{n=1}^{T_{\text{pred}}} \Phi_n (d_{k+n|k}^{\text{comm}}) \\ \text{s.t.} \quad & \tilde{\varepsilon}_{k+n|k} + \eta \le d_{k+n|k}^{\text{comm}} \le \bar{d}^{\text{comm}}, \quad \forall n. \end{aligned} \tag{55}$$

The stage cost function is defined as

$$\Phi_n(d_{k+n|k}^{\text{comm}}) = \frac{w_1}{1 - \exp\Big(-\frac{d_{k+n|k}^{\text{comm}} - \tilde{\varepsilon}_{k+n|k} + \eta}{\sigma} \Big)} + w_2 \left(d_{k+n|k}^{\text{comm}} \right)^2, \tag{56}$$

where $w_1, w_2, \eta, \sigma > 0$ are design parameters.

To analyze convexity, the Hessian matrix of $J_{\text{comm}}(\mathbf{d})$ is diagonal:

$$\nabla^2 J_{\text{comm}}(\mathbf{d}) = \text{diag} \left(\Phi_1'', \ldots, \Phi_{T_{\text{pred}}}'' \right). \tag{57}$$

For notational simplicity, define

$$\gamma_n = \exp\Big(-\frac{d_{k+n|k}^{\text{comm}} - \tilde{\varepsilon}_{k+n|k} + \eta}{\sigma} \Big). \tag{58}$$

Under the constraint $d_{k+n|k}^{\text{comm}} \ge \tilde{\varepsilon}_{k+n|k} + \eta$, the exponent is strictly negative, which implies $0 < \gamma_n < 1$. Therefore, the second-order derivative of each stage cost satisfies

$$\Phi_n''(d_{k+n|k}^{\text{comm}}) = \frac{w_1}{\sigma^2} \frac{\gamma_n (1 + \gamma_n)}{(1 - \gamma_n)^3} + 2w_2 > 2w_2 > 0. \tag{59}$$

Hence,

$$\nabla^2 J_{\text{comm}}(\mathbf{d}) \succeq 2w_2 I \succ 0, \tag{60}$$

which shows that $J_{\text{comm}}(\mathbf{d})$ is strongly convex over the feasible set. With the predicted trajectories fixed, the added safety penalty is a sum of squared positive parts of affine functions of $\mathbf{d}$ and is therefore convex. Hence, the augmented objective $\widetilde{J}_{\text{comm}}(\mathbf{d})$ remains $2w_2$-strongly convex. Provided that $\bar{d}^{\text{comm}} > \tilde{\varepsilon}_{k+n|k} + \eta$ for all n, the feasible set is non-empty, closed, and bounded, and therefore compact. Consequently, the communication margin subproblem admits a unique global minimizer. Algorithm 1 summarizes the alternating updates of the control sequence and communication safety margins.

Algorithm 1 CA-DMPC: Communication-Aware Distributed Model Predictive Control

Input: Prediction horizon T_{pred}, reference trajectory $\tilde{\mathbf{X}}_k^i$, Markov state $\pi_{(k)}^i$, BCD iteration number N_{bcd}, MPC iteration number N_{mpc}
Output: Optimal control input $U_{(k|k)}^{i*}$ and communication margin $\mathbf{d}^*$
for $i \in \mathcal{N}$ **do**
  Transmit nominal trajectory $\bar{\mathbf{X}}_k^i$ at time step k;
  Receive nominal trajectories $\bar{\mathbf{X}}_k^j$, where $j \in \mathcal{N}_i$;
end for
Initialize $j \leftarrow 0$;
while stopping criterion is not satisfied **and** $j < N_{\text{bcd}}$ **do**
  $j \leftarrow j + 1$;
  {— Subproblem 1: Solve for Control U —}
  for $m \leftarrow 1$ to N_{mpc} **do**
    Compute matrices $\mathcal{P}$ and $\mathcal{Q}$ in Eq. (54);
    Solve the QP problem in Eq. (53) to obtain $\mathbf{U}_k^{i*}$;
    Update predicted trajectory $\bar{\mathbf{X}}_k^i$ based on $\mathbf{U}_k^{i*}$;
  end for
  {— Subproblem 2: Solve for $\mathbf{d}$ —}
  Initialize $\pi_{(k|k)}^i \leftarrow \pi_{(k)}^i$;
  for $n \leftarrow 1$ to T_{pred} **do**
    $\pi_{(k+n|k)}^i \leftarrow \pi_{(k+n-1|k)}^i P$;
    $P_{c(k+n|k)}^i \leftarrow \sum_{r=1}^q [\pi_{(k+n|k)}^i]_r$;
    Compute expected spatial uncertainty ε^i
  end for
  Solve subproblem in Eq. (55) and obtain $\mathbf{d}^*$;
end while
Extract the first control input $U_{(k|k)}^{i*}$ from $\mathbf{U}_k^{i*}$;
return $U_{(k|k)}^{i*}$, $\mathbf{d}^*$.

B. Complexity Analysis

Without decomposition, the decision variable dimension of the original nonlinear MPC problem scales linearly with the prediction horizon T_{pred}. Direct solution using general-purpose solvers typically entails a computational complexity of $\mathcal{O}(T_{\text{pred}}^3)$, which poses challenges for meeting the real-time requirements of online vehicular control.

In the proposed BCD framework, the original problem is decoupled into two tractable subproblems:

- Vehicle Control Subproblem: With the communication safety distance fixed, the vehicle dynamics are linearized, yielding a QP problem with sparse structure. The solving complexity is approximately $\mathcal{O}(T_{\text{pred}}^2)$, representing the dominant computational load.
- Communication Safety Distance Subproblem: This problem can be solved independently for each prediction step as a single-variable convex optimization, with a total linear complexity of $\mathcal{O}(T_{\text{pred}})$, which is negligible compared to the control subproblem.

Since the outer BCD loop typically converges within 2–4 iterations, the overall complexity is effectively reduced to $\mathcal{O}(T_{\text{pred}}^2)$. Furthermore, the QP for each vehicle can be executed in parallel, ensuring that the algorithm maintains excellent real-time performance even as the fleet size increases.

C. Convergence and Approximation Analysis

In each outer BCD iteration, the vehicle-control and communication margin blocks are optimized alternately with the other block fixed, so the objective in Eq. (37a) is monotonically non-increasing. Since all objective terms are nonnegative under the selected weighting matrices and parameters, the objective is lower bounded, and its value sequence therefore converges. At each SCP iteration, the nonlinear dynamics and collision-avoidance constraints in Eqs. (37c) and (37d) are linearized around the latest nominal trajectory, yielding an efficiently solvable convex QP. Its solution updates the nominal trajectory, generating numerically consistent iterates and progressively refining the approximation of the original nonconvex subproblem.

Let z stack the predicted states and control inputs, and let $z^{(r)}$ denote the linearization point at SCP iteration r. Since the nonlinear mappings are continuously differentiable with locally Lipschitz continuous gradients, their first-order Taylor expansions satisfy

$$f(z) = f\left(z^{(r)}\right) + \nabla f\left(z^{(r)}\right)^{\top}\left(z - z^{(r)}\right) + \mathcal{O}\left(\|z - z^{(r)}\|^2\right), \tag{61}$$

where $f(\cdot)$ denotes the nonlinear functions in the original subproblem. The approximation error is second order in $\|z - z^{(r)}\|$ and becomes negligible relative to the first-order descent term for sufficiently small SCP updates.

Combined with the monotonic non-increase of the BCD objective, the local consistency and second-order accuracy of SCP yield a convergent objective sequence and stable numerical behavior. Although global optimality cannot be guaranteed due to the intrinsic nonconvexity of the original formulation, the above analysis explains the practical convergence and favorable solution quality observed in the simulations.

VII. Simulations

In this section, we validate the accuracy of the proposed Markov model and demonstrate both the effectiveness and the advantages of the CA-DMPC vehicle control strategy through numerical experiments.

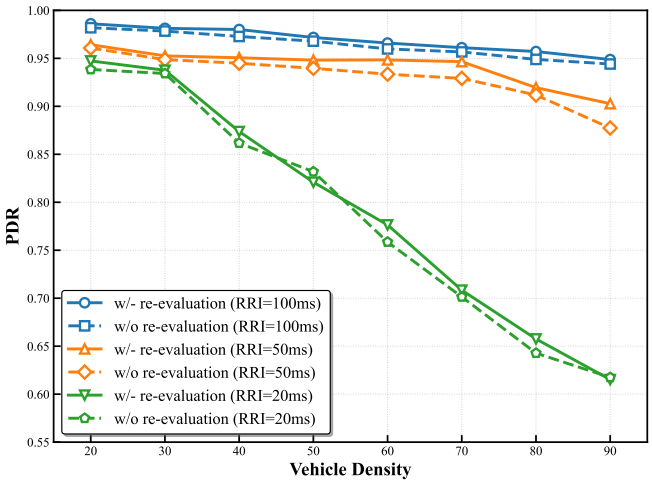

Fig. 6. Comparison of PDR for different resource allocation methods

In the communication simulation, the MAC-layer protocol is implemented in the ns-3 network simulator [47]. The simulation comprehensively accounts for vehicle mobility characteristics, packet transmission demands, the channel model, and the sensing-based resource selection and reservation mechanisms. For the control simulation, a typical ramp-merging scenario was designed, and distributed MPC control of vehicles was implemented using CasADi [48]. The ramp-merging scenario is divided into three zones: the approach zone, the merging zone, and the stabilization zone, with lengths of 100 m, 50 m, and 200 m, respectively. The simulation parameters are listed in Table II.

We first evaluate the effectiveness of incorporating the re-evaluation mechanism into the resource selection process. According to 3GPP specifications, when RRI $\geq$ 100 ms, the RC counter is configured within the range [5, 15]; when RRI $\leq$ 100 ms, the range is adjusted to $[5 \cdot C, 15 \cdot C]$, where $C = 100/\max(20, RRI)$ [49]. Fig. 6 compares the Packet Delivery Ratio (PDR) with and without the re-evaluation mechanism under varying traffic densities. It can be observed that, regardless of traffic density or RRI, the proposed mechanism consistently achieves a higher PDR than the conventional SPS method, with the improvement being particularly notable at an RRI of 50 ms. However, as the RRI decreases and vehicle density increases, the performance gain from the re-evaluation mechanism gradually diminishes. This is attributed to the fact that a shorter RRI combined with higher vehicle density intensifies resource competition and substantially reduces resource availability. Consequently, the probability of re-evaluation failure increases sharply, thereby limiting the potential performance improvement.

We further validated the accuracy of the proposed Markov chain based analytical model. Specifically, the re-evaluation failure probability was obtained under different vehicle densities, and the analytical predictions were compared with simulation results. Fig. 7 illustrates the strong consistency between the theoretical analysis and the simulation results. As vehicle density increases, the failure probability rises significantly due to intensified resource competition in high-

TABLE II
SIMULATION PARAMETERS

parameters	values	parameters	values	parameters	values	parameters	values
Δt	0.1s	Q_X	$\mathrm{diag}\{1,1,0,0\}$	RRI	{100,50,20}	N_{bcd}	2
T_{pred}	30	Q_U	$\mathrm{diag}\{1,0.1\}$	N_{sc}	4	N_{mpc}	3
L_v	3.5m	M_f	$[\mathrm{diag}\{1,0.3\}^T, 0^{2\times2}]$	p_0	0.2	w_1, w_2	0.1
W_v	1.7m	$\overline{U}$	$[7.0, 34°]^T$	$[p,q]$	[5,15],[10,30],[25,75]	ns-3	3.42
K_X	10	$\underline{U}$	$[-7.0, -34°]^T$	μ	0	CasADi	3.7.1
K_U	10	α	8	λ	20∼90	Python	3.11

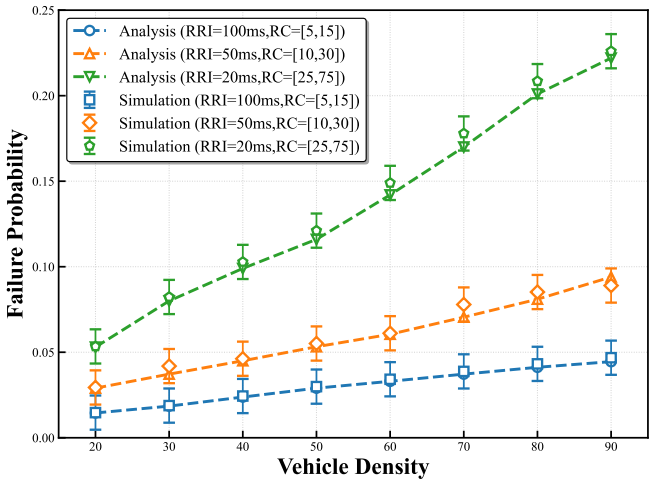

Fig. 7. Comparison of simulation results and analysis results in terms of re-evaluation failure probability

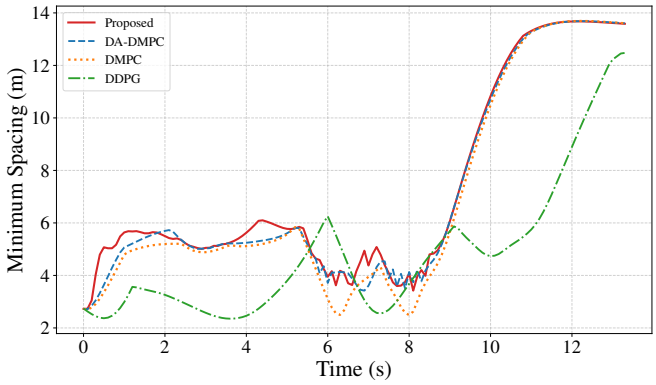

Fig. 8. Minimum distance of vehicles under different algorithms in ramp-merging scenarios.

density traffic scenarios. Under different RRI settings, the failure probability also increases noticeably, with the effect being particularly pronounced when RRI = 20 ms. This is because shorter RRIs lead to a higher transmission frequency within the same time interval, resulting in longer resource occupation and consequently more severe competition, which in turn raises the failure probability. Overall, both the analytical and simulation results fall within one standard deviation, confirming the accuracy and reliability of the proposed Markov model in characterizing communication collision probability.

The proposed CA-DMPC is compared with standard DMPC, delay-aware DMPC (DA-DMPC), and a multi-agent DDPG baseline. The standard DMPC baseline is implemented following the distributed MPC framework in [16]. We implement the DA-DMPC baseline with reference to the delay-aware motion-planning approach in [41]. Specifically, the most recently received neighboring vehicle states are propagated to the current control instant under a constant-velocity assumption before being used in the local MPC. We independently implement a multi-agent DDPG baseline inspired by the DDPG-based merging-control approach in [38]. For the multi-vehicle coordination setting considered here, our implementation uses a shared actor and a centralized critic. Each vehicle outputs longitudinal acceleration and front-wheel steering angle based on its tracking errors, reference trajectory information, and relative states of neighboring vehicles. The reward function accounts for trajectory tracking, safe inter-vehicle spacing, and control smoothness. The actor and critic each contain two hidden layers, with 256 units per layer in the actor and 512 units per layer in the critic. Their learning rates are 10^{-4} and 10^{-3}, respectively, and the training batch size is 256.

Fig. 8 shows that CA-DMPC maintains safe and relatively stable vehicle spacing during merging without excessive conservatism, avoiding sharp reductions in the minimum distance. DMPC and DA-DMPC exhibit larger fluctuations and temporary spacing reductions. DDPG shows greater variability during the critical merging phase, although spacing increases afterward. These results indicate that explicitly accounting for communication uncertainty improves safety compared with neglecting communication impairments or compensating only for delayed information.

Fig. 9 illustrates the evolution of acceleration and steering angle during ramp merging under different control strategies. DMPC exhibits noticeable fluctuations in both control inputs, which may reduce ride comfort. DA-DMPC partially alleviates these fluctuations, although residual oscillations and abrupt changes remain. The DDPG-based method also exhibits oscillatory control inputs across different vehicles. In contrast, the proposed CA-DMPC produces smoother acceleration and steering profiles throughout the merging process. This behavior is consistent with its use of predicted communication states to estimate spatial uncertainty and adapt the safety margin.

Fig. 10 compares the lateral tracking errors of all vehicles under different control strategies during the ramp-merging process. It can be observed that the proposed CA-DMPC maintains relatively small lateral tracking errors for most vehicles throughout the merging process. Although temporary deviations appear during lane-changing maneuvers, the tracking errors quickly converge to values close to zero after merging,

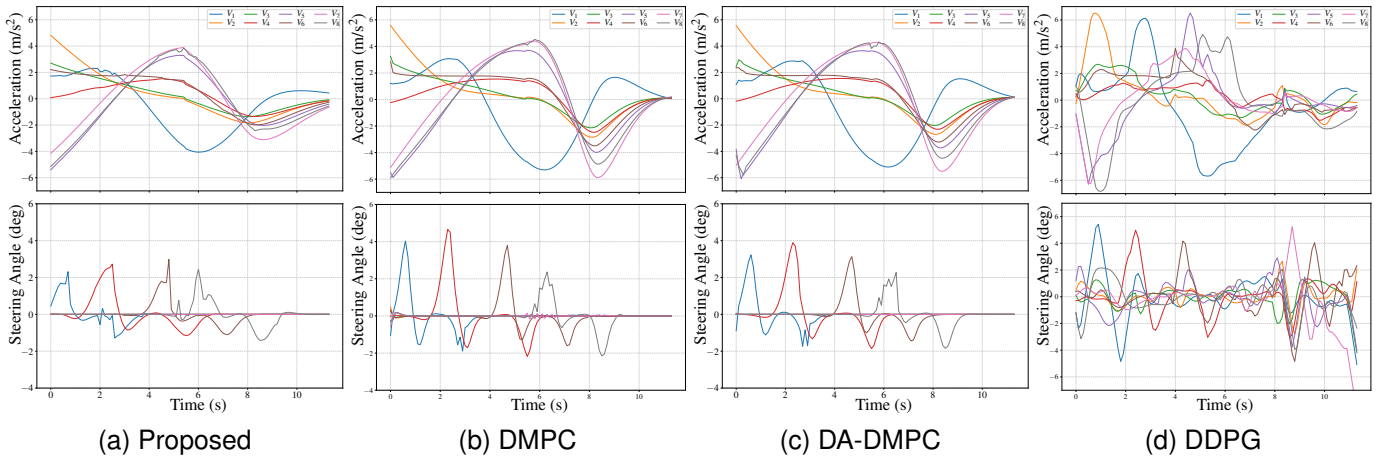

Fig. 9. Steering angle and acceleration of vehicles over time under different algorithms in ramp-merging scenarios.

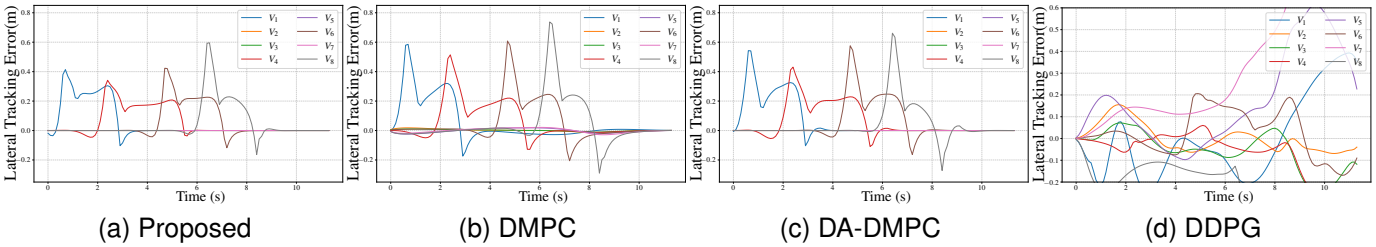

Fig. 10. Lateral tracking error of vehicles over time for different algorithms in ramp-merging scenarios.

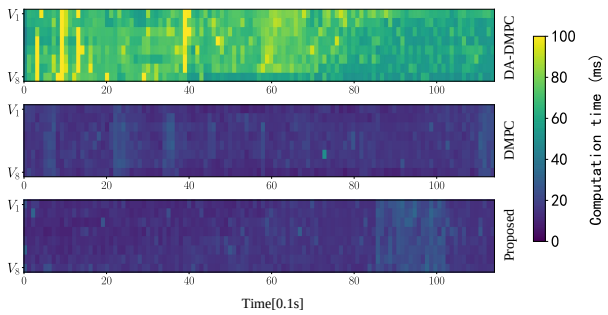

Fig. 11. Computation time under different algorithms in ramp-merging scenarios.

indicating accurate trajectory tracking and stable lateral control performance. The DMPC and DA-DMPC methods exhibit larger transient errors for several vehicles, especially during the critical merging stage. While both methods are able to complete the merging task, noticeable oscillations and delayed error convergence can still be observed. This suggests that ignoring communication uncertainty or only compensating for delayed information is insufficient to guarantee consistently accurate lateral tracking in dynamic merging scenarios. In contrast, the DDPG-based method shows significantly larger tracking deviations and persistent fluctuations over time. Several vehicles fail to converge rapidly after the merging maneuver, indicating reduced control consistency and weaker robustness under multi-vehicle interactions.

Fig. 11 presents the computation time of different control strategies for all vehicles during the ramp-merging process, where each row in the heatmap corresponds to one vehicle and each column represents one control step. It can be observed that the DA-DMPC method exhibits the highest computational burden, with significantly larger solving times and more frequent peaks throughout the simulation horizon. The DMPC achieves lower computational cost than DA-DMPC, but still shows occasional increases during intensive vehicle interactions in the merging stage. In contrast, the proposed CA-DMPC framework maintains relatively low and stable computation time across different vehicles and control steps. This improvement mainly stems from the convexification of the original coupled non-convex problem and the reformulation of the control subproblem into a standard QP problem, which can be solved efficiently by mature optimization solvers. As a result, the proposed method significantly reduces the online computational burden while preserving real-time feasibility. This comparison reports the time required to solve the online MPC optimization problems. DDPG is omitted because it generates control actions through neural network inference.

Fig. 12 compares the average computation time of different control strategies as the number of vehicles increases. All methods require more computation time with more vehicles. DA-DMPC consistently incurs the highest computational cost, followed by standard DMPC. The proposed CA-DMPC maintains the lowest or comparable computation time, with a mild increase as the vehicle population grows, indicating favorable computational scalability in the evaluated scenarios.

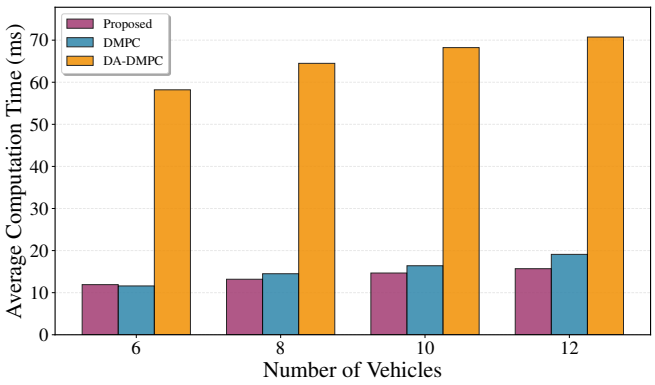

Fig. 12. Average computation time under different algorithms for varying numbers of vehicles in ramp-merging scenarios.

VIII. Conclusion

This paper investigated cooperative ramp merging under imperfect NR V2X communications and proposed a communication-aware distributed MPC framework. An NR V2X Mode 2 Markov model was developed to characterize resource reservation, collision dynamics, and resource re-evaluation. The predicted communication uncertainty was mapped into spatial prediction errors and incorporated into distributed MPC through adaptive safety constraints. The resulting coupled optimization problem was solved through problem decomposition and QP reformulation.

Simulation results demonstrated that the proposed framework achieves smoother control inputs, more stable inter-vehicle spacing, and better trajectory tracking than the benchmark methods. It also maintains competitive computational efficiency as the number of vehicles increases, supporting its effectiveness and computational scalability in the evaluated ramp-merging scenarios.

Small-scale fading may cause additional decoding failures, while correlated shadowing may sustain poor link conditions and increase the likelihood of consecutive packet losses. These effects can prolong the intervals between trajectory updates, potentially causing the current model to underestimate spatial prediction uncertainty and the required safety margin under adverse propagation conditions. Future work will extend the uncertainty model to incorporate reception probabilities that depend on channel conditions and account for temporal correlation in reception failures.

References

[1] Y. Chung and W. W. Recker, "Spatiotemporal analysis of traffic congestion caused by rubbernecking at freeway accidents," *IEEE Trans. Intell. Transp. Syst.*, vol. 14, no. 3, pp. 1416–1422, 2013.

[2] H. Zhou, P. Fan, and J. Li, "Global proportional fair scheduling for networks with multiple base stations," *IEEE Trans. Veh. Technol.*, vol. 60, no. 4, pp. 1867–1879, 2011.

[3] W. Wang *et al.*, "Value matters: A novel value of information-based resource scheduling method for CAVs," *IEEE Trans. Veh. Technol.*, vol. 73, no. 6, pp. 8720–8735, 2024.

[4] S. E. Li *et al.*, "Dynamical modeling and distributed control of connected and automated vehicles: Challenges and opportunities," *IEEE Intell. Transp. Syst. Mag.*, vol. 9, no. 3, pp. 46–58, 2017.

[5] J. Shen *et al.*, "Ringsfl: An adaptive split federated learning towards taming client heterogeneity," *IEEE Trans. Mobile Comput.*, vol. 23, no. 5, pp. 5462–5478, 2024.

[6] Z. Yao, J. Jiang, P. Fan, Z. Cao, and V. O. K. Li, "A neighbor-table-based multipath routing in ad hoc networks," in *Proc. 57th IEEE Veh. Technol. Conf. (VTC Spring)*, vol. 3, Jeju, Korea, 2003, pp. 1739–1743.

[7] C. Meng, K. Xiong, W. Chen, B. Gao, P. Fan, and K. B. Letaief, "Sum-rate maximization in STAR-RIS-assisted RSMA networks: A PPO-based algorithm," *IEEE Internet Things J.*, vol. 11, no. 4, pp. 5667–5680, 2024.

[8] X. Wang *et al.*, "RadioDiff-k^2: Helmholtz equation informed generative diffusion model for multi-path aware radio map construction," *IEEE J. Sel. Areas Commun.*, vol. 44, pp. 2318–2333, 2026.

[9] W. Wang *et al.*, "Optimizing age of information in vehicular edge computing with federated graph neural network multi-agent reinforcement learning," *IEEE Trans. Wireless Commun.*, vol. 25, pp. 23 017–23 032, 2026.

[10] Q. Wu *et al.*, "Large language model-based task offloading and resource allocation for digital twin edge computing networks," *IEEE Trans. Mobile Comput.*, vol. 25, no. 7, pp. 10 290–10 301, 2026.

[11] X. Gu *et al.*, "DRL-based resource allocation for motion blur resistant federated self-supervised learning in IoV," *IEEE Internet Things J.*, vol. 12, no. 6, pp. 7067–7085, 2025.

[12] X. Xu *et al.*, "Velocity-adaptive access scheme for semantic-aware vehicular networks: Joint fairness and AoI optimization," *IEEE Trans. Mobile Comput.*, vol. 25, no. 8, pp. 12 205–12 221, 2026.

[13] Y. Yang and P. Fan, "Doppler frequency offset estimation and diversity reception scheme of high-speed railway with multiple antennas on separated carriage," *J. Mod. Transp.*, vol. 20, no. 4, pp. 227–233, 2012.

[14] M. Ji *et al.*, "Active movable-element RIS assisted vehicular semantic communications: Modeling and optimization," *IEEE Trans. Wireless Commun.*, vol. 25, pp. 20 588–20 605, 2026.

[15] M. Ji *et al.*, "Single-step 6-D movable antenna reconfiguration for high-mobility IoV: Modeling, analysis, and optimization," *IEEE Trans. Wireless Commun.*, vol. 25, pp. 18 499–18 514, 2026.

[16] J. Chu *et al.*, "V2X-assisted distributed computing and control framework for connected and automated CAVs under ramp merging scenario," *IEEE Trans. Mobile Comput.*, vol. 25, no. 5, pp. 7436–7453, 2026.

[17] M. H. C. Garcia *et al.*, "A tutorial on 5G NR V2X communications," *IEEE Commun. Surveys Tuts.*, vol. 23, no. 3, pp. 1972–2026, 2021.

[18] W. Mao, K. Xiong, Y. Lu, P. Fan, and Z. Ding, "Energy consumption minimization in secure multi-antenna UAV-assisted MEC networks with channel uncertainty," *IEEE Trans. Wireless Commun.*, vol. 22, no. 11, pp. 7185–7200, 2023.

[19] X. Xu *et al.*, "Enhanced velocity-adaptive scheme: Joint fair access and age of information optimization in vehicular networks," *IEEE Trans. Mobile Comput.*, vol. 25, no. 3, pp. 3488–3505, 2026.

[20] X. Gu, J. Peng, L. Cai, W. Liu, X. Zhang, and Z. Huang, "Resource reservation coordination for vehicle platooning in C-V2X networks," *IEEE Trans. Wireless Commun.*, vol. 23, no. 6, pp. 5515–5528, 2024.

[21] G. P. Wijesiri N.B.A., J. Haapola, and T. Samarasinghe, "A discrete-time Markov chain based comparison of the MAC layer performance of C-V2X mode 4 and IEEE 802.11p," *IEEE Trans. Commun.*, vol. 69, no. 4, pp. 2505–2517, 2021.

[22] X. Gu *et al.*, "Performance analysis and optimization for semi-persistent scheduling in C-V2X," *IEEE Trans. Veh. Technol.*, vol. 72, no. 4, pp. 4628–4642, 2023.

[23] M. C. Lucas-Estañ *et al.*, "An analytical latency model and evaluation of the capacity of 5G NR to support V2X services using V2N2V communications," *IEEE Trans. Veh. Technol.*, vol. 72, no. 2, pp. 2293–2306, 2023.

[24] V. Todisco, Z. Wu, and A. Bazzi, "Improving NR-V2X autonomous mode through resource re-evaluation," in *Proc. IEEE Veh. Netw. Conf. (VNC)*, Kobe, Japan, 2024, pp. 125–131.

[25] L. Cao, S. Roy, and H. Yin, "Resource allocation in 5G platoon communication: Modeling, analysis and optimization," *IEEE Trans. Veh. Technol.*, vol. 72, no. 4, pp. 5035–5048, 2023.

[26] J. Chen, Y. Zhou, and E. Chung, "An integrated approach to optimal merging sequence generation and trajectory planning of connected automated vehicles for freeway on-ramp merging sections," *IEEE Trans. Intell. Transp. Syst.*, vol. 25, no. 2, pp. 1897–1912, 2024.

[27] J. Rios-Torres and A. A. Malikopoulos, "Automated and cooperative vehicle merging at highway on-ramps," *IEEE Trans. Intell. Transp. Syst.*, vol. 18, no. 4, pp. 780–789, 2017.

[28] K. Hou, F. Zheng, X. Liu, and G. Guo, "Cooperative on-ramp merging control model for mixed traffic on multi-lane freeways," *IEEE Trans. Intell. Transp. Syst.*, vol. 24, no. 10, pp. 10 774–10 790, 2023.

[29] Y. Zhou, M. E. Cholette, A. Bhaskar, and E. Chung, "Optimal vehicle trajectory planning with control constraints and recursive implementation for automated on-ramp merging," *IEEE Trans. Intell. Transp. Syst.*, vol. 20, no. 9, pp. 3409–3420, 2019.

[30] S. Hwang, K. Lee, H. Jeon, and D. Kum, "Autonomous vehicle cut-in algorithm for lane-merging scenarios via policy-based reinforcement learning nested within finite-state machine," *IEEE Trans. Intell. Transp. Syst.*, vol. 23, no. 10, pp. 17 594–17 606, 2022.

[31] Y. Xue, C. Ding, B. Yu, and W. Wang, "A platoon-based hierarchical merging control for on-ramp vehicles under connected environment," *IEEE Trans. Intell. Transp. Syst.*, vol. 23, no. 11, pp. 21 821–21 832, 2022.

[32] Z. Zhang, Q. Wu, P. Fan, N. Cheng, W. Chen, and K. B. Letaief, "DRL-based optimization for AoI and energy consumption in C-V2X enabled IoV," *IEEE Trans. Green Commun. Netw.*, vol. 9, no. 4, pp. 2144–2159, 2025.

[33] D. Chen *et al.*, "Deep multi-agent reinforcement learning for highway on-ramp merging in mixed traffic," *IEEE Trans. Intell. Transp. Syst.*, vol. 24, no. 11, pp. 11 623–11 638, 2023.

[34] S. Hu *et al.*, "AgentsCoMerge: Large language model empowered collaborative decision making for ramp merging," *IEEE Trans. Mobile Comput.*, vol. 24, no. 10, pp. 9791–9805, 2025.

[35] R. Sun, N. Cheng, C. Li, F. Chen, and W. Chen, "Knowledge-driven deep learning paradigms for wireless network optimization in 6G," *IEEE Netw.*, vol. 38, no. 2, pp. 70–78, 2024.

[36] Q. Wu *et al.*, "From LLMs to agentic and embodied AI for next-generation intelligent vehicular communications: A comprehensive survey," *IEEE Commun. Surveys Tuts.*, vol. 28, pp. 6983–7020, 2026.

[37] M. Ji *et al.*, "Joint optimization of trajectory control, resource allocation, and task offloading for multi-UAV-assisted IoV," *IEEE Trans. Mobile Comput.*, vol. 25, no. 9, pp. 15 342–15 359, 2026.

[38] X. Tong, Y. Shi, Q. Zhang, and S. Chen, "Adaptive on-ramp merging strategy under imperfect communication performance," *Veh. Commun.*, vol. 44, p. 100681, 2023.

[39] Y. Fang, H. Min, X. Wu, W. Wang, X. Zhao, and G. Mao, "On-ramp merging strategies of connected and automated vehicles considering communication delay," *IEEE Trans. Intell. Transp. Syst.*, vol. 23, no. 9, pp. 15 298–15 312, 2022.

[40] X. Zhang, S. Fang, Y. Shen, X. Yuan, and Z. Lu, "Hierarchical velocity optimization for connected automated vehicles with cellular vehicle-to-everything communication at continuous signalized intersections," *IEEE Trans. Intell. Transp. Syst.*, vol. 25, no. 3, pp. 2944–2955, 2024.

[41] Z. Li *et al.*, "Edge-assisted V2X motion planning and power control under channel uncertainty," *IEEE Trans. Veh. Technol.*, vol. 72, no. 7, pp. 9641–9646, 2023.

[42] Y. Xie *et al.*, "Resource allocation for twin maintenance and task processing in vehicular edge computing network," *IEEE Internet Things J.*, vol. 12, no. 15, pp. 32 008–32 021, 2025.

[43] A. Molina-Galan, L. Lusvarghi, B. Coll-Perales, J. Gozalvez, and M. L. Merani, "On the impact of re-evaluation in 5G NR V2X mode 2," *IEEE Trans. Veh. Technol.*, vol. 73, no. 2, pp. 2669–2683, 2024.

[44] 3GPP, "NR; medium access control (MAC) protocol specification (release 16)," 3rd Generation Partnership Project (3GPP), Technical Specification (TS) 38.321, Mar. 2021.

[45] S. M. Ross, *A First Course in Probability*. Pearson Harlow, UK, 2020.

[46] C. Brady, L. Cao, and S. Roy, "Modeling of NR C-V2X mode 2 throughput," in *Proc. IEEE Int. Workshop Tech. Committee Commun. Quality Rel. (CQR)*, Arlington, Virginia, USA, 2022, pp. 19–24.

[47] G. F. Riley and T. R. Henderson, "The ns-3 network simulator," in *Modeling and Tools for Network Simulation*. Springer, 2010, pp. 15–34.

[48] J. A. E. Andersson, J. Gillis, G. Horn, J. B. Rawlings, and M. Diehl, "CasADi: A software framework for nonlinear optimization and optimal control," *Math. Program. Comput.*, vol. 11, no. 1, pp. 1–36, 2019.

[49] 3GPP, "TR 37.985 overall description of radio access network (RAN) aspects for vehicle-to-everything (V2X) based on LTE and NR," 3GPP, Tech. Rep. 37.985, September 2020, v16.0.0, Release 16.

Qianju Shen received the B.S. degree from Chengdu University of Technology, Chengdu, China, in 2024. He is currently pursuing the M.S. degree in communication engineering at the School of Automation and Intelligent Science (School of IoT), Jiangnan University, Wuxi, China. His research interests include the Internet of Vehicles, machine learning, and mobile edge computing.

Qiong Wu (Senior Member, IEEE) received the Ph.D. degree in information and communication engineering from National Mobile Communications Research Laboratory, Southeast University, Nanjing, China, in 2016. From 2018 to 2020, he was a postdoctoral researcher with the Department of Electronic Engineering, Tsinghua University, Beijing, China. He is currently an associate professor with the School of Automation and Intelligent Science (School of IoT), Jiangnan University, Wuxi, China.

Dr. Wu is a Senior Member of IEEE and China Institute of Communications. He has published over 120 papers in high impact journals and conferences, and authorized over 30 patents. He was elected as one of the world's top 2% scientists in 2024 and 2022 by Stanford University. He has received the young scientist award of ICCCS'24 and ICITE'24, as well as the best young scholar award of IoTIR'26. He won the high-impact paper of Chinese Journal of Electronics award. He has been awarded the National Academy of Artificial Intelligence (NAAI) Certified AI Senior Engineer and Senior Research Fellow, and was the excellent reviewer of Computer Networks in 2024. He has severed as the editorial board member, early career editorial board member, (lead) guest editor for over 10 journals, as well as the invited speaker, TPC chair, organizing committee chair, publication chair, special session chair, workshop chair, TPC member and session chair for over 30 international conferences. His current research interest focuses on vehicular networks, autonomous driving communication technology, and machine learning.

Pingyi Fan (Senior Member, IEEE) received the B.S. degree in mathematics from Hebei University, Baoding, China, in 1985, the M.S. degree in mathematics from Nankai University, Tianjin, China, in 1990, and the Ph.D. degree in electronic engineering from Tsinghua University, Beijing, China, in 1994. He is currently a professor with the Department of Electronic Engineering, Tsinghua University, where he is also the director of the Open-Source Data Recognition Innovation Center. His research interests include 6G wireless communication networks, semantic and generalized information theory, machine learning, and big-data processing.

He has been a co-recipient of 17 best paper awards, including the IEEE GLOBECOM 2014 Best Paper Award, the IEEE ICC 2020 Best Paper Award, the IEEE ICCCS 2023 and 2024 Best Paper Awards, the IEEE Communications Society TAOS Technical Committee Best Paper Award in 2020, and the IEEE Communications Society Katherine Johnson Best Young Author Paper Award. He currently serves as an associate editor for IEEE Transactions on Cognitive Communications and Networking, vice chair of the Information Theory Branch of the Chinese Institute of Electronics, co-chair of China 6G-ANA TG4, chair of the Network and Communication Technology Committee of IEEE ChinaSIP, and co-chair of the Academic Committee of the NAAI Asia Research Institute. He is a Member of the European Academy of Engineering (EAE), an Academician of the International Eurasian Academy of Sciences (IEAS), a Member of the U.S. National Academy of Artificial Intelligence (NAAI), an IET Fellow, and also an IEICE Overseas Member.

Kezhi Wang (Senior Member, IEEE) received the Ph.D. degree from the University of Warwick, U.K. He is a Professor with the Department of Computer Science, Brunel University of London, U.K. His research interests include wireless communications, mobile edge computing, and machine learning. He is a Clarivate Highly Cited Researcher in 2023-2024.

Wen Chen (Senior Member, IEEE) received the BS and MS degrees from Wuhan University, China, in 1990 and 1993, respectively, and the PhD degrees from the University of Electro-communications, Japan, in 1999. He is currently a tenured professor with the Department of Electronic Engineering, Shanghai Jiao Tong University, China. He is a clarivate highly cited researcher, and fellow of Chinese Institute of Electronics. He is the Shanghai Chapter chair of IEEE Vehicular Technology Society, and vice president of the Shanghai Institute of Electronics. He was the distinguished lecturers of IEEE Communications Society and IEEE Vehicular Technology Society, editors of IEEE Transactions on Wireless Communications and IEEE Transactions on Communications.

Cui Zhang received her Ph.D. degree from Institute of Information Engineering, Chinese Academy of Sciences (CAS) in 2017. From 2017 to 2021, she worked in Huawei 2012 Laboratory for Trustworthy system and Formal Verification research. From 2021 to 2023, she was an expert at security technique of real-time operating system (RTOS) for Intelligent Driving in Banma Network Technology Co. Ltd. Currently she joins Wuxi Institute of Technology. Her main research interests include mobile computing, RTOS, security and formal verification.

Guoqiang Mao (Fellow, IEEE) is a Chair Professor, Director of the Research Center of Frontier Technologies in Intelligent and Connected Transportation, Southeast University. Between 2014 and 2019, he was a Leading Professor, Founding Director of the Research Institute of Smart Transportation, and Deputy Director of the National Key Laboratory of Space-Air-Ground Integrated Service Networks. Before that he was with University of Technology Sydney and the University of Sydney. He has published 300 papers in international conferences and journals that have been cited more than 17,000 times. His H-index is 61 and is in the list of Top 2% most-cited Scientists Worldwide by Stanford University in between 2022 and 2025 both by Single Year and by Career Impact. He serves as a Vice-Director of Smart Transportation Information Engineering Society, Chinese Institute of Electronics (2022-), and was a co-chair IEEE ITS Technical Committee on Communication Networks (2014-2017). He is an editor of the IEEE Transactions on Intelligent Transportation Systems (since 2018), IEEE Transactions on Wireless Communications (2014-2019), IEEE Transactions on Vehicular Technology (2010-2020) and received "Top Editor" award for outstanding contributions to the IEEE Transactions on Vehicular Technology in 2011, 2014 and 2015. He has served as a chair, co-chair and TPC member in a number of international conferences. His research interest includes intelligent transport systems, Internet of Things, wireless localization techniques, mobile communication systems, and applied graph theory and its applications in telecommunications. He is a Fellow of IEEE, AAIA and IET.

Khaled B. Letaief (Fellow, IEEE) received the B.S. (Hons.), M.S., and Ph.D. degrees in electrical engineering from Purdue University, West Lafayette, IN, USA, in 1984, 1986, and 1990, respectively. From 1990 to 1993, he was a Faculty Member with the University of Melbourne, Melbourne, VIC, Australia. Since 1993, he has been with The Hong Kong University of Science and Technology (HKUST). While at HKUST, he has held many administrative positions, including the Head of the Department of Electronic and Computer Engineering, the Director of the Wireless IC Design Center, the Founding Director of the Huawei Innovation Laboratory, and the Director of Hong Kong Telecom Institute of Information Technology. He was a Chair Professor and the Dean of Engineering. Under his leadership, the School of Engineering transformed its education and research scope, produced high-caliber scholarship, and actively pursued knowledge transfer and societal engagement, achieving significant advances in international rankings (rising from November 2009 to November 2015 according to the QS World University Rankings). From 2015 to 2018, he joined Hamad Bin Khalifa University (HBKU) as a Provost to help establish a research-intensive university in Qatar in partnership with strategic institutions, including Northwestern University, Carnegie Mellon University, Cornell University, and Texas A&M University. He has worked as a Consultant for various organizations, including Huawei, ASTRI, ZTE, Nortel, PricewaterhouseCoopers, and Motorola. He is the Internationally Recognized Leader in wireless communications and networks, with research interests in artificial intelligence, big data analytics systems, mobile cloud and edge computing, tactile internet, and 5G systems. His prolific contributions include over publications, which have garnered more than 69,425 citations with a h-index of 116. He holds 15 inventions, including 11 U.S. patents.

Dr. Letaief is a member of the United States National Academy of Engineering, a fellow of Hong Kong Institution of Engineers, and a member of Hong Kong Academy of Engineering Sciences. He has received numerous prestigious awards, including the 2024 IEEE James Evans Avant Garde Award, 2024 Distinguished Purdue University Alumni Award, 2022 IEEE Edwin Howard Armstrong Achievement Award, and 2021 IEEE Communications Society Best Survey Paper Award. He has also received the 2019 Joint Paper Award from the IEEE Communications Society and Information Theory Society, the 2016 IEEE Marconi Prize Award in Wireless Communications, and over 20 IEEE Best Paper Awards. He is well recognized for his service to IEEE and professional societies, where he has held numerous leadership positions, including a Treasurer of the IEEE Communications Society, and an Elected Member of the IEEE Product Services and Publications Board. He served as the Founding Editor-in-Chief of IEEE Transactions on Wireless Communications and has served on the editorial boards of other premier journals, including IEEE Journal on Selected Areas in Communications Special Issue on Wireless Communications Series as the Editor-in-Chief. He also served as the President of the IEEE Communications Society from 2018 to 2019. He is recognized as an ISI Highly Cited Researcher and was listed among the top 30 scholars in the AI 2000 Internet of Things category in 2020.